Tropical Atlantic decadal oscillation and its potential impact on the equatorial atmosphere-ocean dynamics: A simple model study

Sang-Ki Lee[1] and Chunzai Wang[2]

[1] Cooperative Institute for Marine and Atmospheric Studies, University of Miami, Miami FL
[2] Atlantic Oceanographic and Meteorological Laboratory, NOAA, Miami FL

Submitted to Journal of Physical Oceanography
Feb 2007 (2nd revision)

Abstract. Simple coupled atmosphere-ocean models are used to study the potential influence of the tropical Atlantic decadal oscillation on the equatorial Atlantic atmosphere-ocean dynamics. Perturbing the model tropical Atlantic at the extra-tropics (25-30^{o}) with a decadal frequency, inter-hemispheric SST dipole mode emerges due to the Wind-Evaporation-SST feedback. Near the equator, a cross-equatorial oceanic gyre develops due to the dipole-induced wind stress curl. Once formed, this oceanic gyre transports surface water across the equator from the cold to the warm hemisphere in the western boundary region and from the warm to the cold hemisphere in the Sverdrup interior. Interestingly, this occurs during both the positive and negative phases of the dipole oscillation, thus, producing a persistent positive zonal SST gradient along the equator. Bjerknes-type feedback later kicks in to further strengthen the equatorial SST anomaly. Eventually, this feature grows to a quasi-stationary stage sustaining the equatorial westerly wind anomalies; thus, also causing the depression (uplift) of the equatorial thermocline in the east (west), a condition similar to the Atlantic-Niño. The dynamic relationship between the dipole SST oscillation and the equatorial thermocline suggests that a strengthening (weakening) of the dipole mode corresponds to a weakening (strengthening) of the equatorial thermocline slope.

1. Introduction

Unlike the tropical Pacific, climatic fluctuations over the tropical Atlantic are largely forced by perturbations of remote origins, such as El Niño-Southern Oscillation (ENSO) and North Atlantic Oscillation (NAO) (Curtis and Hastenrath, 1995; Nobre and Shukla, 1996; Enfield and Mayer, 1997; Czaja et al. 2002; Enfield et al. 2006). Tropical Atlantic variability (TAV) includes two major modes, namely the Atlantic-Niño and dipole modes (a preferable terminology for the latter is cross-equatorial SST gradient mode, or simply meridional mode, but here we use these terms interchangeably). The first mode is analogous to ENSO in the Pacific and prevails at the interannual time scale, but requires external perturbations to sustain finite-amplitude oscillations (Zebiak, 1993). The second mode, on the other hand, is dominant at the decadal time scale and the associated SST anomaly is most pronounced off the equator around 10-15^{o} latitude bands (Chang et al., 1997; Xie, 1999). Like the Atlantic-Niño mode, the meridional mode is weakly damped (Xie, 1999), thus anti-symmetric configurations of SST anomaly are not ubiquitous in the tropical Atlantic (Enfield et al. 1999). Nevertheless, using a semi-empirical model for the relationship between surface heat flux and SST, Chang et al. (1997) find that the interactions of the ocean and atmosphere through surface heat flux give rise to decadal oscillations of dipole structure similar to observations (*e.g.*, Nobre and Shukla, 1996). Consistent with this finding, Xie (1999) demonstrates clearly that a dipole SST pattern can emerge in a simple coupled atmosphere-ocean model of the tropical Atlantic through the Wind-Evaporation-SST (WES) feedback (Xie and Philander, 1994) if the extra-tropical decadal forcing is sufficiently large. Collectively, these studies suggest that the Atlantic dipole mode is not self-sustaining, thus it is critically dependent upon the extra-tropical forcing patterns. But, many of these studies also suggest that, even in the absence of inter-hemispheric SST anti-correlation, significant (more than 95% confidence) cross-equatorial SST gradients occur frequently (about 50% of the time during 1856-1991 according to Enfield et al. 1999)

and can be associated with climate variability in the tropical Atlantic region (Wang, 2002). A recent Coupled General Circulation Model (CGCM) study by Huang and Shukla (2005) also shows that the WES feedback can prevail in non-dipole configurations, causing mid-latitudinal disturbances to propagate equatorward, in agreement with idealized model studies (Liu, 1996; Xie, 1997). See Xie and Carton (2004) for a complete review on patterns, mechanisms and climate impacts of TAV.

It has been suggested that ocean dynamics do not have a major impact on TAV (Carton et al. 1996; Seager et al. 2001; Alexander and Scott, 2002; Chang et al., 2003; Barreiro et al. 2005; Saravanan and Chang, 2004; Joyce et al. 2004). However, some studies argue that the equatorial Atlantic Ocean dynamics are actively involved in TAV. Servain et al. (1999; 2000), for instance, report that a significant correlation exists between the two tropical Atlantic modes at both the decadal and interannual time scales during 1979-93, and that both modes involve latitudinal displacements of the ITCZ as in the annual response. Murtugudde et al. (2001) present a partially supportive modeling result stressing that the two modes are significantly correlated only for limited record lengths prior to and after 1976. They argue that the correlation falls apart when longer time-series from 1949 to 2000 are considered, due to the large shift in equatorial thermocline depth that occurred in late 1970s. They also argue that the meridional mode is strong prior to the large shift in equatorial thermocline depth but it weakens afterwards, suggesting that the meridional mode is somehow linked to the equatorial Atlantic atmosphere-ocean at the multi-decadal time scale.

These findings of Servain et al. (1999; 2000) and Murtugudde et al. (2001) generate many important questions that deserve further investigations. Among others, one key question that we want to explore in this study is *how the meridional SST oscillation and the equatorial atmosphere-ocean dynamics are potentially tied together at the decadal or longer time scales.* Since the internal variability in the equatorial Atlantic is preferred at the interannual time scale (Zebiak, 1993), it is

unlikely that the meridional mode is significantly affected by the equatorial atmosphere-ocean dynamics at the decadal or longer time scales. Therefore, our working hypothesis is that the equatorial atmosphere-ocean dynamics can be influenced or even controlled by the dipole SST oscillation at the decadal or longer time scales. We test this hypothesis by performing a series of simple coupled model experiments. It will be shown in the following sections that our coupled model experiments indeed support this hypothesis and that the dipole-induced cross-equatorial gyre circulation and the associated nonlinear heat advection play a key role in bridging the meridional SST oscillation and the equatorial atmosphere-ocean dynamics.

The framework of our modeling study closely follows Xie (1999). Here, we revise and extend his model by allowing zonal variations in both the atmosphere and ocean, and replacing the slab ocean model with a fully dynamic 2.5-layer reduced gravity ocean model previously used in Lee and Csanady (1999b).

2. Models

The original Gill (1980) model is used for the atmosphere. The governing equations are written as (unless specified otherwise, all variables are perturbations from their mean states)

$$\varepsilon U - fV = -\frac{\partial P}{\partial x}, \tag{2.1}$$

$$\varepsilon V + fU = -\frac{\partial P}{\partial y}, \tag{2.2}$$

$$\varepsilon P + C^2\left(\frac{\partial U}{\partial x} + \frac{\partial V}{\partial y}\right) = -KT_1, \tag{2.3}$$

where U and V are the zonal and meridional components of lower tropospheric wind perturbation, P is the lower tropospheric pressure anomaly (divided by air density), T_1 is the SST anomaly, f is the

Corioles parameter, C is the internal gravity wave speed, ε is the damping rate and K is the thermal coupling coefficient.

The ocean model is a 2.5-layer reduced gravity model (Lee and Csanady, 1999b) consisting of two active layers, the surface mixed layer and the thermocline layer, on top of the stagnant deep layer. The momentum and continuity equations, linearized from the mean state, can be written as

$$\frac{\partial \mathbf{v}_1}{\partial t} - f\mathbf{k}\times\mathbf{v}_1 = -\frac{1}{\rho_0}\nabla p_1 + \frac{c_d\mathbf{V}}{\rho_0 H_1} + A_h\nabla^2\cdot\mathbf{v}_1, \tag{2.4}$$

$$\frac{\partial \mathbf{v}_2}{\partial t} - f\mathbf{k}\times\mathbf{v}_2 = -\frac{1}{\rho_0}\nabla p_2 + A_h\nabla^2\cdot\mathbf{v}_2, \tag{2.5}$$

$$\frac{\partial h_1}{\partial t} + H_1\nabla\cdot\mathbf{v}_1 = w_e, \tag{2.6}$$

$$\frac{\partial h_2}{\partial t} + H_2\nabla\cdot\mathbf{v}_2 = -w_e, \tag{2.7}$$

where $\mathbf{v}_1$ and $\mathbf{v}_2$ are the anomalous velocity vectors for the two active layers, h_1 and h_2 are the thickness perturbations from their mean values H_1 and H_2, $\mathbf{V}$ is the surface wind perturbation vector, c_d is the drag coefficient and A_h is the horizontal momentum diffusion coefficient. On the basis of the hydrostatic relation, the pressure gradient terms are given by

$$\nabla p_1 = g\alpha\nabla\left[h_1\left(\overline{T}_1 - \overline{T}_3\right) + h_2\left(\overline{T}_2 - \overline{T}_3\right)\right], \tag{2.8}$$

$$\nabla p_2 = g\alpha\nabla\left[\left(h_1 + h_2\right)\left(\overline{T}_2 - \overline{T}_3\right)\right], \tag{2.9}$$

where α is the thermal expansion coefficient, $\overline{T}_1$, $\overline{T}_2$ and $\overline{T}_3$ are mean state temperatures of the two active layers and the deep inert layer, respectively. The anomalous vertical entrainment rate, w_e, is parameterized as linearly dependent on the mixed layer depth anomaly, h_1:

$$w_e = -\gamma h_1, \tag{2.10}$$

where the vertical mixing coefficient γ is set to $(365\text{day})^{-1}$. It is reasonable to assume that the entrainment rate is proportional to the mixed layer depth anomaly (h_1) because upwelling (uplift of isotherms) brings the isotherms and cold subsurface water closer to the surface where turbulent mixing is greater, thus increases the rate of entrainment cooling in the mixed layer (Lee et al., 2007). Such equation form is, thus commonly used in many simple ocean models (*e.g.*, McCreary and Kundu, 1998; McCreary and Yu, 1992). It is also important to note that this equation is used for estimating anomalous entrainment rate, not the total. Since the detrainment rarely occurs in the tropical oceans, a negative value does not necessarily mean detrainment, but it rather means a reduction of entrainment rate due to the deepening of mixed layer.

The thermodynamic equation for the mixed layer, which is used to compute the SST anomaly (T_1), can be written as

$$\frac{\partial T_1}{\partial t} + \left(\underbrace{\overline{\mathbf{v}}_1 \cdot \nabla T_1}_{\text{(a1)}} + \underbrace{\mathbf{v}_1 \cdot \nabla \overline{T}_1}_{\text{(a2)}} + \underbrace{\mathbf{v}_1 \cdot \nabla T_1}_{\text{(a3)}} \right) = \frac{\overline{Q}_e}{c_p \rho_0 H_1} \left(\frac{\overline{U}U + \overline{V}V}{\overline{U}^2 + \overline{V}^2} \right) - rT_1 \\ \underbrace{-\frac{\overline{w}_e}{H_1} T_1}_{\text{(b1)}} \underbrace{-\frac{w_e}{H_1}(\overline{T}_1 - \overline{T}_2)}_{\text{(b2)}} \underbrace{-\frac{w_e}{H_1} T_1}_{\text{(b3)}} + A_T \nabla^2 T_1 + F, \tag{2.11}$$

where the overbar denotes the mean state variable, c_p is the specific heat of sea water, r is the thermal damping coefficient, A_T is the thermal diffusion coefficient, $\overline{Q}_e$ is the latent heat flux of the mean state (positive downward), $\overline{U}$ and $\overline{V}$ are the zonal and meridional surface wind component of the mean state, respectively, and F is the external forcing to be described later. Note that the temperatures of the lower layers remain constant (*i.e.*, $T_2 = T_3 = 0$), thus no additional equation is needed for the thermocline layer. The three terms inside the bracket on the lhs of (2.11) are advective heat flux divergence terms. They are (a1) the advection of anomalous temperature gradient by mean flow, (a2) the advection of mean temperature gradient by anomalous flow and (a3) the nonlinear advective heat

flux divergence, respectively. The first term on the rhs of (2.11) is obtained by linearizing the bulk formula for latent heat flux (see Liu, 1996 and Xie, 1999 for detailed derivation), and it is the central component for the WES feedback to occur in the coupled model. The second term on the rhs is the thermal damping term arising from temperature dependence of latent heat flux. The next three are the vertical mixing terms. They are (b1) the vertical mixing due to mean upwelling, and (b2) the linear and (b3) nonlinear portion of the anomalous vertical mixing. The last two terms in the rhs of (2.11) are the thermal diffusion and external forcing.

The model Atlantic Ocean domain is a rectangular box, extending zonally from 80^{o}W to 20^{o}E and meridionally from 30^{o}S to 30^{o}N with the model resolution of about 0.7^o. The north and south boundaries are closed with a slip-condition applied at all sidewalls. The Gill atmospheric model also extends from 30^{o}S to 30^{o}N, but it is a global model in zonal direction with a periodic boundary condition. The mean ocean state is 200m deep (H_1=100m; H_2=100m) with the thermal parameters chosen to yield two internal gravity wave speeds of 2.5 and 1.0 ms^{-1}. All model parameters and their values used in this study are listed in Table 1. These values in the table are chosen to be identical to those used in Xie (1999) except for two parameters, namely the thermal coupling coefficient, K, and the thermal damping coefficient, r. The values for these two variables are appropriately chosen to ensure that the simulated WES feedback is weakly damped in the tropical Atlantic model configuration with an intrinsic resonant period at approximately 10 years, as indicated in previous observational and modeling studies.

In order to mimic the decadal extra-tropical perturbations typically caused by the NAO, SST perturbations are imposed only between 25^o and 30^o in both hemispheres, with the forcing period of 10 years. Coupled model runs are carried out using an anti-symmetric extra-tropical forcing pattern, *i.e.*,

the sign of forcing is opposite in the two hemispheres but with the same amplitude, thus the forcing term F in (2.11) is given by

$$F = \begin{cases} \kappa \cdot \cos(2\pi/10\text{yrs} \cdot t) & \text{for } y = 25^{\circ}\text{N} - 30^{\circ}\text{N} \\ 0 & \text{for } y = 25^{\circ}\text{S} - 25^{\circ}\text{N} \\ -\kappa \cdot \cos(2\pi/10\text{yrs} \cdot t) & \text{for } y = 25^{\circ}\text{S} - 30^{\circ}\text{S}, \end{cases} \tag{2.12}$$

where κ is set to $1^{\circ}C\ (365\text{day})^{-1}$.

Seven primary experiments are carried out with and without the thermodynamic terms that involve ocean dynamics (a1, a2, a3, b1, b2 and b3 in 2.11) as shown in Table 2. In the first five experiments, it is assumed that the mean state is motionless and has a constant mixed layer temperature, thus the three terms that involve the mean state (a1, a2, and b1) all vanish. In the first experiment (Case-1), the Gill atmospheric model is coupled to a so-called slab ocean model. In this case, the three remaining terms that involve ocean dynamics (a3, b2, and b3) are thus neglected in (2.11). In the second experiment (Case-2), (a3) the nonlinear advective heat flux divergence is included while the vertical mixing terms (b2 and b3) are neglected. In the third experiment (Case-3), only (b2) the linear portion of the vertical mixing is included whereas in the fourth experiment (Case-4) only (b3) the nonlinear portion is included. In both Case-3 and Case-4, (a3) the nonlinear advection term is excluded. In the fifth experiment (Case-5), the three terms that involve ocean dynamics (a3, b2 and b3) are included. Two more experiments are carried out to address the potential impact of spatially varying mean state. In one experiment (Case-6), the three terms that involve the mean state (a1, a2 and b1) are included while all other ocean dynamic terms (a3, b2, and b3) are neglected. In the other experiment (Case-7), all six thermodynamic terms that involve ocean dynamics (a1, a2, a3, b1, b2 and b3) are included.

In all of these experiments, the WES feedback (*i.e.*, the first term on the rhs of 2.11), thermal damping, thermal diffusion and forcing terms are retained. In the following section, these seven

coupled model runs under the anti-symmetric extra-tropical forcing (2.12) are used to describe the potential impact of the dipole oscillation on the equatorial Atlantic atmosphere-ocean system.

3. Results

a. Thermally coupled experiment (*Case*-1)

The first experiment (Case-1) is performed by coupling the Gill atmosphere with the slab ocean model (*i.e.*, all six terms that involve ocean dynamics are neglected in 2.11). Fig. 1(a), (b) and (c) show the latitude-time structure of the zonally averaged SST anomaly and wind anomaly components, respectively. The structure of the solution closely resembles the WES feedback mode studied earlier (Xie, 1999), showing clearly the SST see-saw pattern north and south of the equator that slowly propagates equatorward, and the cross-equatorial winds blowing from the cold to the warm hemisphere. As explained by Liu (1996), the equatorial propagation can be understood as follows. A warm SST anomaly in the tropics produces a westerly wind anomaly on the equator side and an easterly wind anomaly on the poleward side. The westerly wind anomaly reduces the mean trade wind speed while the easterly wind anomaly increases the mean wind speed. Accordingly, the related latent heat flux anomaly induces warming on the equator side and cooling on the poleward side, thus causing the warm SST anomaly to propagate toward the equator.

Fig. 1(d), (e) and (f) show the latitude-time structure of the zonally averaged mixed layer depth anomaly and surface ocean current anomaly components corresponding to the wind stress forcing shown in Fig. 1(b) and (c). Note that the ocean anomalies shown here are simply forced by the dipole-induced wind stress; thus, they are not actively involved in the atmosphere-ocean coupling. The mixed layer depth anomaly (h_1) and the SST anomaly (T_1) are negatively correlated, with the former lags the later by about 3 ~ 4 years; thus, the mixed layer depth is more likely to be shallower in the warm

hemisphere and deeper in the cold hemisphere, in agreement with earlier studies (*e.g.*, Joyce et al., 2004). The zonal transport anomaly (u_1H_1), which has the maximum amplitude around 5^o, is mainly controlled by the Sverdrup dynamics. The net cross-equatorial transport anomaly (v_1H_1) is, on the other hand, entirely related to the divergent flow governed by the continuity equation. Generally, it is in the direction from the warming (*i.e.*, $\partial T_1/\partial t > 0$) hemisphere to the cooling hemisphere (*i.e.*, $\partial T_1/\partial t < 0$). It is intersting to note that the cross-equatorial transport, ranging between about ±4 Sv (this is estimated by assuming that the zonal scale of the equatorial Atlantic basin is about 5×10^3 km), is quite significant compared to the mean (about 10 Sv according to Lee and Csanady, 1999a). Therefore, this result poses an intersting hypothesis that the Atlantic meridional overturning circulation is, at least partly, regulated by the dipole oscillation at the decadal time scale. The cross-equatorial gyre transport and the related ocean dynamics are explored further in the later part of this section.

Fig. 2(a) shows the two-dimensional structure of SST and wind anomalies averaged for the positive phase (warm in the north and cold in the south), and Fig. 2(b) for the negative phase (cold in the north and warm in the south) between the model year 21 and 30. As shown in Fig. 2(c), the dipole index used for the phase averaging is the area-averaged SST anomaly of the northern hemisphere minus that of the southern hemisphere. It is important to notice that the model solution is not a standing oscillation: the model solution propagates toward the equator, as shown in Fig. 1, but the propagating solution is averaged out in Fig. 2. The structure of the oscillating solution shown in Fig 2(a) and (b) is very similar to the zonally uniform solution of Xie (1999), but anomalous SST and winds are more pronounced toward the west. As previously noted by Xie (1996), this feature appears to originate from westward propagating WES waves that amplify as they move westward.

Fig. 2(d) and (e) display oceanic mixed layer depth (h_1) and transport (u_1H_1 and v_1H_1) anomalies averaged between the model year 21 and 30 for the negative phase (shallow in the north and deep in

the south), and for the positive phase (deep in the north and shallow in the south), respectively. As shown in Fig. 2(f), the dipole index used for the phase averaging is the area-averaged mixed layer depth anomaly of the northern hemisphere minus that of the southern hemisphere. As discussed earlier, the mixed layer depth anomaly (h_1) is negatively correlated with the SST anomaly (T_1), thus the mixed layer depth is more likely to be shallower in the warm hemisphere and deeper in the cold hemisphere. However, the most striking feature in Fig. 2(d) and (e) is the cross-equatorial gyre circulation that emerges due to the dipole-induced wind stress curl pattern (Joyce et al. 2004). Obviously, this gyre circulation plays no role in this case because the thermodynamic terms associated with ocean dynamics are all turned off. However, it will be shown in the next experiment (Case-2) that when (a3) the nonlinear oceanic heat advection term is activated in the thermodynamic equation (2.11), this gyre circulation allows a cross-equatorial transport of the mixed layer water from the cold to the warm hemisphere in the western boundary region and from the warm to cold hemisphere in the Sverdrup interior, thus, producing a positive SST gradient along the equator. But, before we move on to the next section, it is worthwhile to explore the ocean dynamic processes that are responsible for the net cross-equatorial transport oscillation shown in Fig. 1(f). Note that the Ekman transport, $v_{ekm} = c_d U (\rho_o f H_1)^{-1}$, is a significant portion of the net cross-equatorial transport as shown in Fig. 3(a), but the non-Ekman transport is stronger than the Ekman transport as illustrated in Fig. 3(b). Interestingly, the non-Ekman transport is about 90^o out of phase with the Ekman transport, suggesting that the non-Ekman transport is an ocean dynamic response that tends to compensate the inter-hemispheric mass-imbalance caused by the Ekman transport.

In the classical model of a wind-driven gyre circulation in a closed domain, the meridional mass transport in the Sverdrup interior is exactly balanced by the reverse transport in the western boundary region; thus, the net meridional mass transport below the Ekman layer vanishes at all latitudes (*e.g.*,

Munk, 1950). However, as correctly pointed by Csanady (1986), the so-called "leak-proof" wind-driven gyre circulation models hide some important details of the wind-driven flow, notably the mass balance between wind drift in a surface Ekman layer and the non-Ekman transport below. Since the classical wind-driven model does not explain the net non-Ekman cross-equatorial transport shown in Fig. 3(b), here we use the framework of the so-called *cross-gyre transport solution* of Csanady (1986). Following this framework, the mixed layer transport is decomposed into nonvortical (potential flow) and nondivergent (solenoidal flow) components:

$$u_1 H_1 = \frac{\partial \phi_1}{\partial x} - \frac{\partial \psi_1}{\partial y}, \qquad v_1 H_1 = \frac{\partial \phi_1}{\partial y} + \frac{\partial \psi_1}{\partial x}, \tag{3.1}$$

where ϕ_1 is the transport potential and ψ_1 is the stream function. The divergence and curl of transport can be written as

$$\nabla^2 \phi_1 = -H_1 \left(\frac{\partial u_1}{\partial x} + \frac{\partial v_1}{\partial y} \right), \qquad \nabla^2 \psi_1 = H_1 \left(\frac{\partial v_1}{\partial x} - \frac{\partial u_1}{\partial y} \right), \tag{3.2}$$

The boundary conditions are $\partial\phi/\partial\mathbf{n} = 0$ and $\psi = 0$ at all side walls, where $\mathbf{n}$ is the unit vector normal to each sidewall. With these boundary conditions, the two Poisson equations (3.2) can be solved using the method of successive over relaxation, given the divergence and vorticity from the model output. By definition, the solenoidal flow component ($v_{sol}H_1=\partial\psi_1/\partial x$) contributes nothing to the net cross-equatorial transport, thus the net cross-equatorial transport shown in Fig. 1(f) is exclusively due to the potential flow component ($v_{pot}H_1=-\partial\phi_1/\partial y$).

Fig. 4(a) and (b) show the stream function (ψ_1) and solenoidal flow ($u_{sol}H_1$ and $v_{sol}H_1$) anomalies for the mixed layer averaged between the model year 21 and 30 for the positive phase, and the negative

phase, respectively. The dipole index used for the phase averaging is the area-averaged zonal solenoidal transport anomaly ($u_{sol}H_1$) of the northern hemisphere minus that of the southern hemisphere as shown in Fig. 4(c). A close inspection of Fig. 4(a) and (b) along with Fig. 2(d) and (e) indicates that the oceanic response to the dipole-induced wind stress forcing can be largely explained by using the classical theory of a nondivergent wind-driven gyre circulation (Munk, 1950).

Fig. 4(d) and (e) display transport potential (ϕ_1) and potential flow ($u_{pot}H_1$ and $v_{pot}H_1$) anomalies for the mixed layer averaged between the model year 21 and 30 for the positive phase and the negative phase, respectively. As shown in Fig. 4(f), the dipole index used for the phase averaging is the area-averaged transport potential anomaly of the northern hemisphere minus that of the southern hemisphere. Two striking features are noted. First, the potential flow has no boundary current component. Second, the cross-equatorial potential flow is 90^o out of phase with the solenoidal flow meaning that, when the potential flow is maximized, the cross-equatorial gyre circulation disappears (or change the sign of rotation) and vice versa.

The main lesson in the work of Csanady (1986) is that cross-gyre transport is needed to satisfy the mass imbalance caused by the Ekman transport, and that the net cross-gyre transport involves strictly nonvortical flows, thus, it is usually concealed in the classical wind-driven circulation models. The dynamics of potential flow in this case are somewhat different from the original cross-gyre transport solution, which is applicable only for steady state flows. Thus, in the original cross-gyre transport model, Ekman pumping is the only source of divergence that drives the potential flow. In this case, however, two additional sources of divergence are the local rate of change of the mixed layer depth and the entrainment from the thermocline layer, as clearly indicated in the continuity equation of mixed layer (2.6). A consorted influence of the three divergence sources determines the amplitude and phase of net cross-equatorial transport.

In summary, this experiment (Case-1) confirms that extra-tropical perturbations could cause meridional SST oscillation in the tropical Atlantic through thermodynamic feedback (Xie, 1999), and that the dipole-induced wind forcing could drive a cross-equatorial gyre circulation (Joyce et al., 2004). Further analyses show that the dipole oscillation produces a significant net cross-equatorial transport, thus it may have some effect on the Atlantic meridional overturning circulation. The cross-gyre transport solution of Csanady (1986) provides a useful insight to explain the wind-driven ocean dynamics that regulate the net cross-equatorial mass transport.

b. The role of oceanic heat advection (*Case*-2)

In the next experiment (Case-2), a coupled model run is performed by including (a3) the nonlinear advective heat flux divergence term in the thermodynamic equation (2.11). Fig. 5(a) and (b) are the same as in Fig 2(a) and (b) but for the Case-2. The dipole index used for the phase averaging is the area-averaged SST anomaly of the northern hemisphere from that of the southern hemisphere, as shown in Fig 5c (thin solid line). The most striking departure from the previous experiment is the infiltration of the warm hemisphere into the cold hemisphere in the interior ocean, and the opposite trend in the western boundary region. As a result, a positive (negative) zonal SST anomaly gradient persists in the western (eastern) equatorial ocean during both the positive and negative phases of the dipole oscillation.

The broken line in Fig. 5(c) indicates the area-averaged zonal transport of the northern hemisphere minus that of the southern hemisphere. If this is used as the index for cross-equatorial gyre circulation, a negative (positive) index value represents an anti-clockwise (a clockwise) circulation. A close inspection of the two indices in Fig. 5(c) indicates that during the positive dipole phase between the model year 22 and 26, the cross-equatorial gyre is an anti-clockwise in the first year, but it switches to

a clockwise circulation for the remaining 4 years. Hence, a clockwise cross-equatorial gyre circulation prevails during the positive SST dipole phase. Similarly, an anti-clockwise cross-equatorial gyre circulation prevails during the negative SST dipole phase. As a result, the cross-equatorial gyre circulation transports mixed layer water from the cold to the warm hemisphere in the western boundary region and from the warm to the cold hemisphere in the Sverdrup interior. Since this occurs during both the positive and negative phases of the dipole oscillation, a persistent cold anomaly is produced in the western boundary region and a warm anomaly in the Sverdrup interior. Another noticeable feature in Fig. 5(a) and (b) is the zonal shifts of the SST anomaly maximum (eastward) and minimum (westward). Again, the heat advection by the cross-equatorial gyre circulation is accountable for this model feature: in association with the cross-equatorial gyre circulation, the westward current anomaly in the cold hemisphere pushes the SST anomaly minimum toward west while the eastward current anomaly in the warm hemisphere carries the SST anomaly maximum toward the east.

An important implication of these results is that, when ocean dynamics (nonlinear heat advection in particular) are allowed to participate in the dipole oscillation, a shift may occur in the zonal structure of the equatorial atmosphere and ocean. To better describe the equatorial shift and the associated role of nonlinear oceanic heat advection, it is useful to look at the time-averaged model solution: shown in Fig. 6(a) are the two-dimensional structures of SST and wind anomalies averaged for one full cycle of the dipole oscillation between the model year 21 and 30. The positive SST anomaly in the central equatorial ocean is due to the cross-equatorial gyre circulation and the related meridional heat advection as discussed earlier. The wind anomaly pattern is a typical Gill atmosphere response to an isolated heating source at the central equatorial ocean: a damped atmospheric Kelvin wave along the equator with the zonal wind converging toward the heating source, and a damped atmospheric Rossby wave off the equator (Gill, 1980).

Fig. 6(b) shows mixed layer depth (h_1) and transport (u_1H_1 and v_1H_1) anomalies averaged for the same period between the model year 21 and 30. The shallow thermocline depth and eastward transport anomalies in the western equatorial ocean are consistent with the westerly wind anomaly there. It is important to note that the changes in the thermocline depth do not make direct impact on the SST anomaly because the vertical mixing terms (b1, b2 and b3) are all excluded in this experiment; thus, the equatorial positive feedback, also known as Bjerknes feedback (Bjerknes, 1969), does not play any role here.

Heat advection is neither a source nor a sink of thermal energy, because it merely redistributes thermal energy between different geographic locations. Accordingly, the amplitude and phase of the dipole oscillation are minimally affected by the oceanic heat advection as it becomes clear by comparing the dipole index of this experiment (Fig. 5(c)) with that of the previous experiment (Fig. 2(c)). Nevertheless, the cross-equatorial gyre circulation and the related heat advection generate some interesting model features, in particular the expansion of the warm hemisphere into the cold hemisphere in the Sverdrup interior and vice versa in the western boundary region. A warm SST anomaly is then created in the central equatorial ocean, and it persists during both the positive and negative phases of the dipole oscillation. In turn, this equatorial SST anomaly forces the Gill atmosphere to produce westerly wind anomaly in the western equatorial ocean. In response to this wind anomaly, the shallow thermocline depth and eastward transport anomalies prevail in the western equatorial ocean. Since the vertical mixing is turned off, the Bjerknes feedback does not play a role in this experiment.

c. The role of vertical mixing (*Case*-3 *and Case*-4)

Two experiments are carried out to understand how the vertical mixing influences the dipole oscillation. In one experiment (Case-3), only (b2) the linear vertical mixing term is included in the thermodynamic equation (2.11), and in the other experiment (Case-4), only (b3) the nonlinear vertical mixing term is included. Note that (b1) the vertical mixing of the mean state is assumed zero (*i.e.*, $\overline{w}_e = 0$) in these two experiments.

Fig. 7 is the same as in Fig. 1 but for Case-3. When the model solution is compared to the thermally coupled case (Case-1), it is noted that the amplitude of dipole oscillation is reduced considerably (note that different contour intervals are used in Fig. 1 and Fig. 7), suggesting that the mixed layer depth oscillation and the related linear vertical mixing contribute to a negative feedback. The dynamics responsible for this negative feedback is very straightforward. Fig. 7(a) and (d) reveal that the mixed layer depth anomaly (h_1) is negatively correlated with the SST anomaly (T_1) without much time lag; thus, the mixed layer depth is shallower in the warm hemisphere and deeper in the cold hemisphere. Because the linear vertical mixing is proportional to the mixed layer depth anomaly (see 2.10), it tends to cool down the warm hemisphere and to warm up the cold hemisphere, a negative feedback mechanism. The two-dimensional structure of the model solution for Case-3 is very similar to as in Fig. 2, but with much reduced amplitude, thus, it is not shown here.

In the next experiment (Case-4), (b3) the nonlinear vertical mixing term is included in the thermodynamic equation (2.11) instead of (b2) the linear vertical mixing term. Fig. 8 is the same as in the left column of Fig. 2 but for Case-4. In comparison to the thermally coupled case (Exp-1), one distinctive feature in Fig. 8 is that the cold hemisphere is intensified while the warm hemisphere is weakened. Fig 8(c) clearly shows that the SST and mixed layer depth anomalies are negatively correlated, with no apparent time lag. Therefore, (b3) the nonlinear vertical mixing, which is proportional to $T_1 h_1$ (see 2.10), contributes to a cooling in both hemispheres; thus, weakening the warm

hemisphere and strengthening the cold hemisphere during both the positive and negative phases of the dipole oscillation.

While the horizontal heat advection term is excluded in this experiment, the structure of the model solution shares two important features of the Case-2 (Fig. 5). First, the SST minimum is pushed against the western boundary while the SST maximum is shifted to the east. To explain this feature, it is important to recognize that the amplitude of mixed layer depth anomaly is pronounced off the western boundary due to beta effect (Stommel, 1948). Therefore, the nonlinear vertical mixing and the related cooling are also maximized off the western boundary region causing weakening (strengthening) of the SST maximum (minimum) there. This explains why the SST minimum is pushed against the western boundary while the SST maximum is shifted to the east. Another important feature to note is that the cold hemisphere infiltrates the warm hemisphere in the western side of model ocean, and vice versa in the interior equatorial ocean. A heat budget analysis suggests that the horizontal heat diffusion is responsible for causing the expansion of the cold hemisphere into the warm hemisphere in the western side of the model ocean where the predominance of the cold hemisphere is most pronounced (not shown). Fig. 9, which is the same as in Fig. 6 but for Case-4, further shows that the nonlinear vertical mixing together with the heat diffusion produces a positive zonal SST gradient along the equator causing a westerly wind anomaly over the central equatorial ocean. This equatorial wind anomaly in turn causes the mixed layer deepening in the eastern equatorial ocean. Near the western boundary, cold SST anomalies prevail because the cold hemisphere predominates the warm hemisphere there. This also explains why the easterly wind anomaly persists in the western boundary region.

In summary, we find that the linear vertical mixing tends to decrease the amplitude of dipole oscillation. But, the equatorial system is undisturbed by the linear vertical mixing. The nonlinear vertical mixing, on the other hand, does influence the equatorial system, and the characteristics of the

model solution are surprisingly similar to those with (a3) the nonlinear oceanic heat advection. In particular, the nonlinear vertical mixing produces a positive zonal SST gradient and a westerly wind anomaly along the equator. The predominance of the cold hemisphere to the warm hemisphere is another noticeable impact of the nonlinear vertical mixing.

d. The role of ocean dynamics (*Case*-5)

So far, we have been exploring the individual role of (a3) nonlinear heat advection, (b2) linear vertical mixing and (b3) nonlinear vertical mixing in the dipole oscillation by performing three coupled model experiments that allow only one of the three processes in each experiment. However, since these ocean dynamic processes coexist in reality, we next explore the role of the integrated ocean dynamics in the dipole oscillation by performing a fully coupled model experiment (Case-5) – the three ocean dynamic terms (a3, b2 and b3) in the thermodynamic equation (2.11) are included in this experiment. In all our previous model experiments, the coupled simulations arrive at their equilibriums after about 10 years or so. In this fully coupled case, however, the basin-averaged energy grows for an extended period of more than several decades until the model reaches a quasi-equilibrium stage.

Before we explore why the fully coupled system takes longer time to adjust, it is helpful to first look at the two-dimensional structure of the solution: Fig. 10 is the same as in the left column of Fig. 2 but for Case-5. In comparison to the thermally coupled case (Case-1), the off-equatorial amplitude of the dipole oscillation is significantly reduced as in Case-3, apparently due to the damping effect of linear vertical mixing. As in Case-2 and Case-4, the positive zonal SST gradient persists in the western and central equatorial oceans due to the influence of (a3) nonlinear heat advection and (b3) nonlinear vertical mixing. In fact, it appears that the fully coupled model experiment (Case-5) contains all the major characteristics of Case-2, Case-3 and Case-4, indicating that all three ocean dynamic processes,

i.e., the nonlinear heat advection (Case-2), linear vertical mixing (Case-3) and nonlinear vertical mixing (Case-4), work more or less independently. But, this conclusion does not apply in the eastern basin where the strong warm SST anomaly prevails with its maximum centered at the equator. Since the warm SST anomaly persists during both the positive and negative phases of the dipole oscillation, it is useful to look at the time-averaged model solution: Fig. 11 is the same as in Fig. 9 but for this experiment (Case-5). It is apparent that the equatorial SST anomaly has much larger amplitude than those shown in Fig. 6 (Case-2) or Fig. 9 (Case-4), and it is most intense in the eastern equatorial ocean. The presence of an intensified equatorial SST anomaly indicates that a positive feedback is at work and it tends to amplify the positive zonal SST gradient along the equator, which is originally caused by the nonlinear heat advection and nonlinear vertical mixing. The westerly wind and deepened thermocline anomalies in the eastern equatorial ocean suggest that the Bjerknes feedback plays an important role.

Further insight can be gained by using the following analogical model for the eastern equatorial SST anomaly, T_o:

$$\frac{dT_o}{dt} = aT_o - bT_o + c\,. \tag{3.3}$$

The first term in the rhs represents positive feedback with the growth rate a, mainly the Bjerknes feedback. The second term represents damping processes that limit the growth of instabilities (negative feedback), such as Newtonian damping. The third term represents the tendency (rate) of the fully coupled model to create a positive zonal SST gradient anomaly along the equator, thus c is always positive. The solution to equation 3.3 is given by (the initial condition is $T_o = 0$)

$$T_o = \frac{c}{b-a}(1-\exp[-(b-a)t])\,. \tag{3.5}$$

It is important to note that the damping rate is always larger than the growth rate, *i.e.*, $b - a > 0$, because the coupled system is always stable. Therefore, the equilibrium solution ($T_o = c/(b - a)$; $t \rightarrow \infty$) is

always a warm anomaly, and its magnitude depends critically on the damping rate minus growth rate, (b - a). This solution also explains that an e-folding time of $(b - a)^{-1}$ is required for the system to adjust to the final equilibrium stage. In this particular experiment (Case-5), the e-folding time is about several decades, but it varies with different parameter values that affect a, b and c.

In summary, the dipole-induced cross-equatorial gyre circulation and the related heat advection (together with the nonlinear vertical mixing) are directly responsible for inducing the positive zonal SST gradient along the equator, and the subsequent atmosphere-ocean positive feedback further intensifies the zonal SST gradient anomaly, eventually creating a condition similar to the Atlantic-Niño. Once the coupled system reaches its equilibrium stage, the equatorial SST anomaly structure becomes nearly stationary, feeding its energy from the WES feedback that in turn requires decadal perturbations from extra-tropics. Since the Bjerknes feedback in the Atlantic is a damped mode, a continuous forcing is required for the stationary Atlantic-Niño to maintain its strength; thus, the core mechanism can be referred to as a *forced Bjerknes feedback*.

e. The influence of oceanic mean state (*Case-*6 *and Case-*7)

It is assumed in the earlier experiments that the mean state is motionless and has a constant mixed layer temperature, thus the three thermodynamic terms that involve the mean state (a1, a2, and b1) do not play any role. We now want to test how the WES feedback and its impact on the equatorial atmosphere-ocean as discussed in the previous sections are affected when a spatially varying mean state is included in the thermodynamic equation. To address these points, two experiments are performed. In one experiment (Case-6), the three thermodynamic terms that involve the mean state (a1, a2 and b1) are included, while all other ocean dynamic terms (a3, b2, and b3) are neglected. In the

other experiment (Case-7), all of the six thermodynamic terms that involve ocean dynamics are included.

As shown in Fig. 12, the mixed layer temperature of the mean state varies from 23°C at the northern and southern boundaries to 27°C at the equator:

$$\overline{T_1} = 25^{\circ}\mathrm{C} + 2\cos(\pi y / 30^{\circ}). \tag{4.1}$$

The zonal flow component of the mean state is obtained by using Ekman balance with linear damping r_m (= 2.2×10^{-6} $\sec^{-1}$) as in Clement et al. (2005):

$$\overline{u_1} = \frac{r_m c_d \overline{U} + f\overline{V}}{\rho H_1 (f^2 + r^2)}. \tag{4.2}$$

As indicated in Table 1, $\overline{U}$ = –6.5 m s^{-1}, $\overline{V}$ = 0 m s^{-1} and c_d = 0.01 N s m^{-3}, thus we get $\overline{u_1}(y=0)$ = 0.3 m s^{-1}, which is a reasonable value. The meridional flow component of the mean state is more complicated because we also need to consider the geostropic flow component, which has a hemispheric asymmetry. According to Lee and Csanady (1999b), the northward transport of the tropical Atlantic mixed layer water is about 11 Sv (at 8°N) on an annual average, with roughly 10 Sv coming from the equatorial entrainment of upper thermocline layer and the remaining 1 Sv (at 8°S) from the mixed layer water of the South Atlantic. In order to reflect the asymmetric meridional flow structure, we construct our mean state in the following manner. First, we assume that the entrainment rate of the mean state has a Gaussian structure:

$$\overline{w_e} = w_o \exp(-y^2 / m^2), \tag{4.3}$$

where m is a meridional scale, typically 150 km. The scale of the entrainment rate, w_o, is obtained by constraining that the area-integrated entrainment rate is about 10 Sv. Thus, we get $w_o = 3\times10^{-6}$ m s^{-1}, which is a reasonable value. The total meridional velocity (Ekman and geostrophic components) can be now computed by integrating the continuity equation from the southern boundary ($y = y_s$):

$$\overline{v}_1 = \frac{1}{H_1}\left(V_s + \int_{y_s}^{y} \overline{w}_e dy\right), \tag{4.4}$$

where V_s is the meridional volume transport at the southern boundary (=1 Sv). Obviously, the real mean state of the tropical Atlantic Ocean has much more complex structure (Lee and Csanady, 1999a). However, we will not consider the real mean state here, since it is beyond the scope of our simple model study (thus it is left for future study). After performing the two experiments (Case-6 and Case-7) using the above mean state, we find that adding the mean state in the thermodynamic equation tends to stabilize the dipole oscillation. One apparent reason is that (b1) the vertical mixing by the mean state acts as a Newtonian damping around the equator. The same two experiments are repeated after slightly increasing the thermal coupling coefficient, K, from 1.0×10^{-3} to 1.2×10^{-3}m^2 s^{-3} K^{-1}. The model results discussed below are based on the experiments with the increased K value.

Fig. 13 shows the two-dimensional structure of SST and wind anomalies averaged for (a) the positive and (b) negative phases obtained from Case-6. When compared to Case-1, it is apparent that the SST and wind anomalies are stronger in the South Atlantic than in the North Atlantic during both the positive and negative phases. After performing several more experiments with and without one of the three mean state terms (a1, a2 and b1), we find that the advection of anomalous temperature gradient by meridional mean flow is mainly responsible for the pronounced damping in the North Atlantic. It appears that the strong northward advection of anomalous temperature gradient by mean flow tends to interfere with the southward propagation of the SST anomalies and the associated WES feedback in the North Atlantic. In the South Atlantic, on the other hand, the meridional flow of the mean state is much weaker and slightly northward, thus the WES feedback is more or less free from the impact of mean state.

Note that the advection of anomalous temperature gradient by meridional mean flow, $-\overline{v}_1 \partial T_1/\partial y$, always warms (cools) the equatorial ocean during a negative (positive) dipole phase because $\overline{v}_1$ is always northward in this case. And, since $|\partial T_1/\partial y|$ is stronger in the west than in the east along the equator (see earlier discussion in section 3(a) about the possible role of the westward propagating WES waves), the warming (cooling) is also stronger in the west during a negative (positive) dipole phase. As a result, a positive (negative) zonal SST gradient is generated along the equator during a positive (negative) dipole phase. But, it appears that the zonal SST gradient is not robust enough to evoke a Bjerknes feedback in this case.

When all of the six terms involving ocean dynamics (a1, a2, a3, b1, b2, and b3) are included in the thermodynamic equation (Case-7), we find that the model solution has a quite complex structure, but the core dynamics involving the WES feedback and its impact on the equatorial atmosphere-ocean is more or less the same as in the experiment without the mean state (Case-5). We also find that the mean state used in this study is unstable because the simulated anomalies grow almost indefinately. It appears that our coupled model lacks the non-linear mechanisms that typically stabilize unstable systems, but further study is needed to understand why the mean state is unstable. Fig. 14 shows the two-dimensional structures of (a) SST and wind anomalies, and (b) the mixed layer depth and transport anomalies, all averaged for one full cycle of the dipole oscillation between the model year 26 and 35. Note that the anomalies grow indefinately nearly doubling their amplitudes at about year 40, but their spatial structures are unchanged. The warm SST and deep mixed layer depth anomalies in the eastern equatorial basin indicate a stationary Atlantic-Niño condition as in Fig. 11 (Case-5). The model solution is not entirely symmetrical to the equator. As discussed earlier for Case-6, this is due to the meridional flow of the mean state, which is always northward.

In summary, we find that the mean state of the tropical Atlantic Ocean has a large impact on the WES feedback and the equatorial atmosphere-ocean dynamics. In particular, the strong northward mean flow in the North Atlantic Ocean reduces the strength of dipole oscillation by interfering with the southward propagation of the SST anomalies that fuels the WES feedback. As a result, the SST and wind anomalies are stronger in the South Atlantic than in the North Atlantic during both the positive and negative phases. We also find that the WES feedback and its interaction with the equatorial atmosphere-ocean still cause a stationary Atlantic-Niño when the mean state is allowed to interact in the coupled model.

5. Summary and Discussions

Motivated by observations that the two tropical Atlantic climate modes (the zonal and meridional modes) are potentially related at the decadal time scale, we carry out a series of simple coupled model runs to understand the underlying physics, and our findings can be summarized as follows. Perturbing the model tropical Atlantic at the extra-tropics (25-30^{o}) with a decadal frequency, inter-hemispheric SST dipole mode emerges due to the WES feedback. Near the equator, a cross-equatorial gyre circulation develops due to the dipole-induced wind stress curl. This gyre circulation transports equatorial surface water from the cold to the warm hemisphere in the western boundary region and from the warm to the cold hemisphere in the Sverdrup interior. Since this occurs during both positive and negative phases of the dipole oscillation, a positive zonal SST gradient persists along the equator (the nonlinear vertical mixing also contributes to the positive zonal SST gradient). Bjerknes feedback later kicks in to strengthen the equatorial SST anomaly. This feature eventually grows to a quasi-stationary stage sustaining the equatorial westerly wind anomalies, thus, also causing the depression

(uplift) of the equatorial thermocline in the east (west), a condition similar to the Atlantic-Niño. Fig. 15 is a sketch that illustrates this mechanism of the dipole oscillation inducing a stationary Atlantic-Niño.

Adding an idealized mean state in the thermodynamic equation tends to reduce the overall amplitude of anomalies, particularly in the North Atlantic where the strong northward mean flow interferes with the WES feedback. It appears that the mean state does not affect *the forced Bjerknes feedback* because the dipole oscillation still produces a stationary Atlantic-Niño. Nevertheless, further studies are needed to better understand how the real mean state of the tropical Atlantic Ocean affects the dipole oscillation and the equatorial atmosphere-ocean dynamics. Although not shown here, additional experiments are performed with different extra-tropical forcing patterns. We find that the WES feedback mechanism still works under a symmetric extra-tropical forcing with and without ocean dynamics, but the oscillations are much weaker. The stationary Atlantic-Niño that prevails under the anti-symmetric extra-tropical forcing does not exist in that case. On the other hand, if the extra-tropical forcing is confined in the northern or southern hemisphere only, the stationary Atlantic-Niño does develop but with much reduced growth rate. These results suggest that inter-hemispheric SST contrast is the precondition for generating the stationary Atlantic-Niño.

Murtugudde et al (2001) reported two important characteristics of the tropical Atlantic decadal variability in the past 50 years. First, the main mode of tropical Atlantic SST variability changes during the 1970s from a meridional SST gradient mode to a zonal mode. Second, this change is accompanied by a large thermocline shift that strengthens the zonal slope of equatorial Atlantic thermocline. According to our coupled model experiments, a strengthening (weakening) of the dipole mode corresponds to a weakening (strengthening) of the equatorial thermocline slope; thus, suggesting that the shift of equatorial Atlantic thermocline that occurred in 1970s may be due to the concurrent weakening of the dipole mode.

The main conclusion of this study is that the equatorial atmosphere-ocean can be affected by the extra-tropical forcing through the atmosphere-ocean coupling (both thermal and dynamic) and that the ocean dynamics plays a crucial role in bridging the dipole oscillation and the equatorial system. Another potentially important finding of this study is that the dipole oscillation produces a significant net cross-equatorial transport. This suggests that the dipole oscillation may affect the overall strength of the Atlantic meridional overturning circulation. Obviously, we fully recognize the limitations of our coupled model particularly in the aspect of over-simplifying the complex tropical Atlantic system where both the remotely forced and internally generated signals are mixed together. Therefore, our next task is to validate our conclusions using observation data and more sophisticated models. Finally, we want to point out one practical implication of our findings. It is well known that the global CGCMs surfer from a warm SST bias persisting in the eastern equatorial Atlantic Ocean. Based on our findings in this study, one can speculate that the Atlantic dipole oscillation in CGCMs may be too active thus leading to an abnormally large stationary Atlantic-Niño condition. The first step to test this idea is to diagnose whether the dipole oscillation in CGCMs is more active than in the observations.

Acknowledgements. This research was supported by a grant from NOAA Climate Program Office and by the base funding of NOAA/AOML. We are indebted to D. Enfield for many scientific discussions and encouragement. Comments from D. Enfield, A. Mestas-Nuñez, R. Molinari and A. Clement help improve the manuscript. We also thank two anonymous reviewers for their useful suggestions, which led to a significant improvement of the paper. The findings and conclusions in this report are those of the authors and do not necessarily represent the views of the funding agency.

References

Alexander, M., and J. Scott, 2002: The influence of ENSO on air-sea interaction Atlantic, Geophys. Res. Lett.. 29, doi: 10.1029/2001GL014347.

Barreiro, M., P. Chang, L. Ji, R. Saravanan and A. Giannini, 2005: Dynamical elements of predicting boreal spring tropical Atlantic sea-surface temperatures, Dyn. Atmos. Oceans, 39, 61-85.

Bjerknes, J., 1969: Atmospheric teleconnections from the equatorial Pacific. Mon. Wea. Rev., 97, 163-172.

Carton, J. A., X. H. Cao, B. S. Giese, and A. M. da Silva, 1996: Decadal and interannual SST variability in the tropical Atlantic Ocean. J. Phys. Oceanogr., 26, 1165-1175.

Chang, P., L. Ji, and H. Li, 1997: A decadal climate variation in the tropical Atlantic Ocean from thermodynamic air-sea interactions. Nature, 385, 516-518.

Chang, P., L. Ji, and R. Saravanan, 2001: A hybrid coupled model study of tropical Atlantic variability. J. Climate, 14, 361-390.

Chang, P., R. Saravanan, and L. Ji, 2003: Tropical Atlantic Seasonal Predictability: the Roles of El Niño remote influence and thermodynamic air-sea feedback. Geophys. Res. Lett., 30, 1501-1504.

Clement, A. C., R. Seager, and R. Murtugudde, 2005: Why are there tropical warm pools? J. Climate, 18, 5294-5311.

Csanady, G. T., 1986: Cross-gyre transports. J. Phys. Oceanogr., 16, 1703-1711.

Curtis, S. and S. Hastenrath, 1995: Forcing of anomalous sea surface temperature evolution in the tropical Atlantic during Pacific warm events. J. Geophys. Res., 100, 15835-15847.

Czaja, A., P. Van der Vaart, and J. Marshall, 2002: A diagnostic study of the role of remote forcing in tropical Atlantic variability. J. Climate, 15, 3280-3290.

Enfield, D. B. and D. A. Mayer, 1997: Tropical Atlantic sea surface temperature variability and its relation to El Niño-Southern Oscillation. J. Geophys. Res., 102, 929-945.

Enfield, D. B., A. M. Mestas-Nuñez, D. A. Mayer, and L. Cid-Serrano, 1999: How ubiquitous is the dipole relationship in tropical Atlantic sea surface temperatures? J. Geophys. Res., 104, 7841-7848.

Enfield, D. B., S.-K. Lee, and C. Wang, 2006: How are large Western Hemisphere Warm Pools formed? Prog. Oceanogr., 70, 346-365.

Gill, A. E., 1980: Some simple solutions for heat-induced tropical circulation. Quart. J. Roy. Meteor. Soc., 106, 447–462.

Huang, B. and J. Shukla. 2005: Ocean-Atmosphere Interactions in the Tropical and Subtropical Atlantic Ocean. J. Climate 18, 1652-1672.

Joyce, T. M., C. Frankignoul, J. Yang, H.E. Phillips, 2004: Ocean response and feedback to the SST dipole in the Tropical Atlantic. J. Phys. Oceanogr., 34, 2525-2540

Lee, S.-K., G. T. Csanady, 1999a: Warm water formation and escape in the upper tropical Atlantic Ocean: 1. A Literature Review, J. Geophys. Res., 104, 29,561 - 29,571.

Lee, S.-K., G. T. Csanady, 1999b: Warm water formation and escape in the upper tropical Atlantic Ocean: 2. A numerical model study, J. Geophys. Res., 104, 29,573 - 29,590.

Lee, S.-K., D. B. Enfield and C. Wang, 2007: What drives seasonal onset and decay of the Western Hemisphere Warm Pool? J. Climate, In press.

Liu, Z. 1996: Modeling Equatorial Annual Cycle with a Linear Coupled Model. J. Climate, 9, 2376-2385.

McCreary, J. P. and P. K. Kundu, 1988: A numerical investigation of the Somali current during the Southwest Monsoon, J. Mar. Res., 46, 25-58.

McCreary, J. P. and Z. Yu, 1992: Equatorial dynamics in a 2.5 layer model, Prog. Oceanogr., 29, 61-132.

Munk, W. H., 1950: On the wind driven ocean circulation., J. Meteor., 7, 79-93.

Murtugudde, R. G., J. Ballabrera-Poy, J. Beauchamp, A. J. Busalacchi, Relationship between zonal and meridional modes in the tropical Atlantic, Geophys. Res. Lett., 28(23), 4463-4466, 10.1029/2001GL013407, 2001.

Nobre, P. and J. Shukla, 1996: Variations of sea surface temperature, wind stress and rainfall over the tropical Atlantic and South America. J. Climate, 9, 2464-2479.

Saravanan, R. and P. Chang, 2004: Thermodynamic coupling and predictability of tropical sea surface temperature, In Earth Climate: The Ocean-Atmosphere Interaction, C. Wang, S.-P. Xie and J.A. Carton (eds.), Geophys. Monogr., 147, AGU, Washington D.C., 171-180.

Seager, R., Y. Kushnir, P. Chang, N. Naik, J. Miller and W. Hazeleger, 2001. Looking for the role of the ocean in tropical Atlantic decadal climate variability, J. Climate, 14, 638-655.

Servain, J. Jr., A. Dessier, Relationship between the equatorial and meridional modes of climatic variability in the tropical Atlantic, Geophys. Res. Lett., 26(4), 485-488, 10.1029/1999GL900014, 1999.

Servain, J. Jr., I. Wainer, H. L. Ayina, and H. Roquet, 2000. The relationship between the simulated climatic variability modes of the tropical Atlantic, Internat. J. Clim,. 20, 939 – 953.

Stommel, H., 1948: The westward intensification of wind-driven ocean currents. Trans. Am. Geophys. Union, 29, 202-206.

Wang, C., 2002. Atlantic climate variability and its associated atmospheric circulation cells, J. Climate, 15, 1516 – 1536.

Xie, S.-P., and S.G.H. Philander, 1994: A coupled ocean-atmosphere model of relevance to the ITCZ in the eastern Pacific, Tellus, 46A, 340-350.

Xie, S.-P., 1996: Westward propagation of latitudinal asymmetry in a coupled ocean-atmosphere model. J. Atmos. Sci., 53, 3236-3250.

Xie, S.-P., 1997: Unstable Transition of the Tropical Climate to an Equatorially Asymmetric State in a Coupled Ocean-Atmosphere Model. Mon. Wea. Rev., 125, 667-679.

Xie, S.-P., 1999: A dynamic ocean-atmosphere model of the tropical Atlantic decadal variability. J. Climate, 12, 64-70.

Xie, S.-P. and J. A. Carton, 2004: Tropical Atlantic variability: Patterns, mechanisms, and impacts. Earth Climate: The Ocean-Atmosphere Interaction, C. Wang, S.-P. Xie and J.A. Carton (eds.), Geophys. Monogr., 147, AGU, Washington D.C., 121-141.

Zebiak, S. E., 1993. Air-sea interaction in the equatorial Atlantic region, J. Climate, 6, 1567 – 1586.

Table 1. Model parameters and their values used for model integrations. ATM indicates parameters used for the atmospheric model, OCN for the ocean model and CPL for the atmosphere-ocean coupling, respectively.

Parameter	Notation	Value
ε^{-1}	inverse of damping rate (ATM)	2 days
K	thermal coupling coefficient (ATM)	1×10^{-3} m^2 s^{-3} K^{-1}
C	internal gravity wave speed (ATM)	45 m s^{-1}
$\overline{U}$	zonal wind speed of the mean state (ATM)	-6.5 m s^{-1}
$\overline{V}$	meridional wind speed of the mean state (ATM)	0 m s^{-1}
A_h	Laplacian mixing coefficient for momentum (OCN)	4000 m^2 s^{-1}
ρ_0	density of sea water (OCN)	1020 kg s^{-1}
c_p	specific heat of water (OCN)	4200 m s^{-2} K^{-1}
α	thermal expansion coefficient (OCN)	2.5×10^{-4} K^{-1}
γ^{-1}	inverse of vertical mixing coefficient (OCN)	1 year
H_1	thickness of the mixed layer (OCN)	100 m
H_2	thickness of the thermocline layer (OCN)	100 m
$\overline{T}_1$	mean state temperature of the mixed layer (OCN)	25^{o}C
$\overline{T}_2$	mean state temperature of the thermocline layer (OCN)	20^{o}C
$\overline{T}_3$	mean state temperature of the deep motionless layer (OCN)	15^{o}C
$\overline{Q}_e$	latent heat flux of the mean state (positive downward) (CPL)	-100 W m^{-2}
r^{-1}	inverse of thermal damping coefficient (CPL)	2 years
c_d	drag coefficient (CPL)	1×10^{-2} N s m^{-3}
A_T	Laplacian mixing coefficient for heat (CPL)	2000 m^2 s^{-1}
κ	extra-tropical forcing coefficient (CPL)	1 year

Table 2. List of seven primary experiments

Experiment	Ocean dynamic terms included in the thermodynamic equation (2.11)	Mean state of the ocean
Case-1	None	Uniform SST & No flow
Case-2	(a3) Nonlinear advection	Uniform SST & No flow
Case-3	(b2) Linear vertical mixing	Uniform SST & No flow
Case-4	(b3) Nonlinear vertical mixing	Uniform SST & No flow
Case-5	(a3) Nonlinear advection (b2) Linear vertical mixing (b3) Nonlinear vertical mixing	Uniform SST & No flow
Case-6	(a1) Advection of anomalous SST gradient by mean flow (a2) Advection of mean SST gradient by anomalous flow (a3) Vertical mixing by the mean state	Variable SST & Variable flow
Case-7	(a1) Advection of anomalous SST gradient by mean flow (a2) Advection of mean SST gradient by anomalous flow (a3) Nonlinear advection (b1) Vertical mixing by the mean state (b2) Linear vertical mixing (b3) Nonlinear vertical mixing	Variable SST & Variable flow

Figure captions

Figure 1. Case-1: Latitude-time structure of the zonally averaged (a) SST, (b) zonal wind, (c) meridional wind, (d) mixed layer depth, (e) zonal mixed layer transport and (f) meridional mixed layer transport anomalies. The unit is ^{o}C for the SST, ms^{-1} for the wind components, m for the mixed layer depth and m^2s^{-1} for the mixed layer transport components.

Figure 2. Case-1: Two-dimensional structure of SST and wind anomalies averaged for (a) the positive phase and (b) the negative phase are shown in the left column. The dipole index used for the phase averaging is the area-averaged SST of the northern hemisphere minus that of the southern hemisphere as shown in (c). The mixed layer depth and transport anomalies averaged for (d) the negative phase and (e) the positive phase are shown in the right column. The dipole index used in this case is the area-averaged mixed layer depth of the northern hemisphere minus that of the southern hemisphere as shown in (f). The maximum wind is about 1.3 m s^{-1}, and the maximum zonal mixed layer transport is about 9.5 m^2s^{-1}.

Figure 3. Case-1: Latitude-time structure of the zonally averaged meridional (a) Ekman transport and (b) non-Ekman transport components. The unit is m^2s^{-1}. Ekman transport is not defined at the equator, thus it is interpolated at the equator.

Figure 4. Case-1: The stream function (ψ_1) and solenoidal flow ($u_{sol}H_1$ and $v_{sol}H_1$) anomalies for the mixed layer averaged for (a) the positive phase and (b) the negative phase are shown in the left column. The dipole index used for the phase averaging is the area-averaged zonal solenoidal transport

($u_{sol}H_1$) of the northern hemisphere minus that of the southern hemisphere as shown in (c). The transport potential (ϕ_1) and potential flow ($u_{pot}H_1$ and $v_{pot}H_1$) anomalies for the mixed layer averaged for (d) the positive phase and for (e) the negative phase are shown in the right column. The dipole index used in this case is the area-averaged transport potential anomaly of the northern hemisphere minus that of the southern hemisphere as shown in (f). The unit is 10^{-6} m^3s^{-1} for the stream function and transport potential, and m^2s^{-1} for the solenoidal flow and potential flow components. The maximum transport value is about 9.4 m^2s^{-1} for the solenoidal flow component, and about 0.9 m^2s^{-1} for the potential flow component.

Figure 5. Case-2: Two-dimensional structure of SST and wind anomalies averaged for (a) the positive phase and (b) the negative phase. The dipole index used for the phase averaging is the area-averaged SST of the northern hemisphere minus that of the northern hemisphere as shown in (c). The broken line in (c) is the area-averaged zonal transport of the northern hemisphere minus that of the southern hemisphere, and this index is used for cross-equatorial gyre circulation: a negative value indicates a cyclonic circulation and a positive value indicates a clockwise circulation. The maximum wind is about 1.3 ms^{-1}.

Figure 6. Case-2: The two-dimensional structures of (a) SST and wind anomalies, and (b) the mixed layer depth and transport anomalies, all averaged for one full cycle of the dipole oscillation between the model year 21 and 30. The maximum wind is about 0.4 ms^{-1}, and the maximum zonal mixed layer transport is about 3.2 m^2s^{-1}.

Figure 7. Same as in Fig. 1 but for Case-3. Note that the contour intervals are different from those used in Fig. 1.

Figure 8. Same as in the left column of Fig. 2 but for Case-4. The broken line in (c) is the area-averaged mixed layer depth of the northern hemisphere minus that of the southern hemisphere. The maximum wind is about 1.4 ms^{-1}.

Figure 9. Same as in Fig. 6 but for Case-4. The maximum wind is about 0.3 ms^{-1}, and the maximum zonal mixed layer transport is about 2.5 m^2s^{-1}.

Figure 10. Same as in Fig. 8 but for Case-5. The maximum wind is about 0.8 ms^{-1}.

Figure 11. Same as in Fig. 9 but for Case-5. The maximum wind is about 0.4 ms^{-1}, and the maximum zonal mixed layer transport is about 5.2 m^2s^{-1}.

Figure 12. The mixed layer temperature (^oC), zonal mixed layer velocity (in m s^{-1}), meridional mixed layer velocity (in 10 m s^{-1}) and entrainment rate (in 10^5 m s^{-1}) of the mean state used for Case-6 and Case-7. See text for how these values are derived.

Figure 13. Same as in Fig. 8 but for Case-6. The maximum wind is about 1.2 ms^{-1}.

Figure 14. Same as in Fig. 9 but for Case-7. The maximum wind is about 0.4 ms^{-1}, and the maximum zonal mixed layer transport is about 5.3 m^2s^{-1}.

Figure 15. Sketch of the mechanism by which the positive zonal SST gradient is induced along the equator during (a) the positive and (b) negative phases of the Atlantic dipole oscillation. Thicker arrows indicate wind perturbations associated with the dipole oscillation. Dark shades are used for warm SST anomalies and light shades for cold SST anomalies. W-D represents a warm and deep anomaly; W-S a warm and shallow anomaly; C-D a cold and deep anomaly; and C-S a cold and shallow anomaly. Closed circuits represent cross-equatorial gyre circulation that brings the tropical surface water toward the equator. This gyre circulation supplies cold water in the western boundary layer and warm water in the Sverdrup interior during both the positive and negative phases of the dipole oscillation. The warm equatorial SSTA is then shifted to the east and intensified as a result of the Bjerknes feedback, thus, producing a stationary Atlantic-Niño condition.

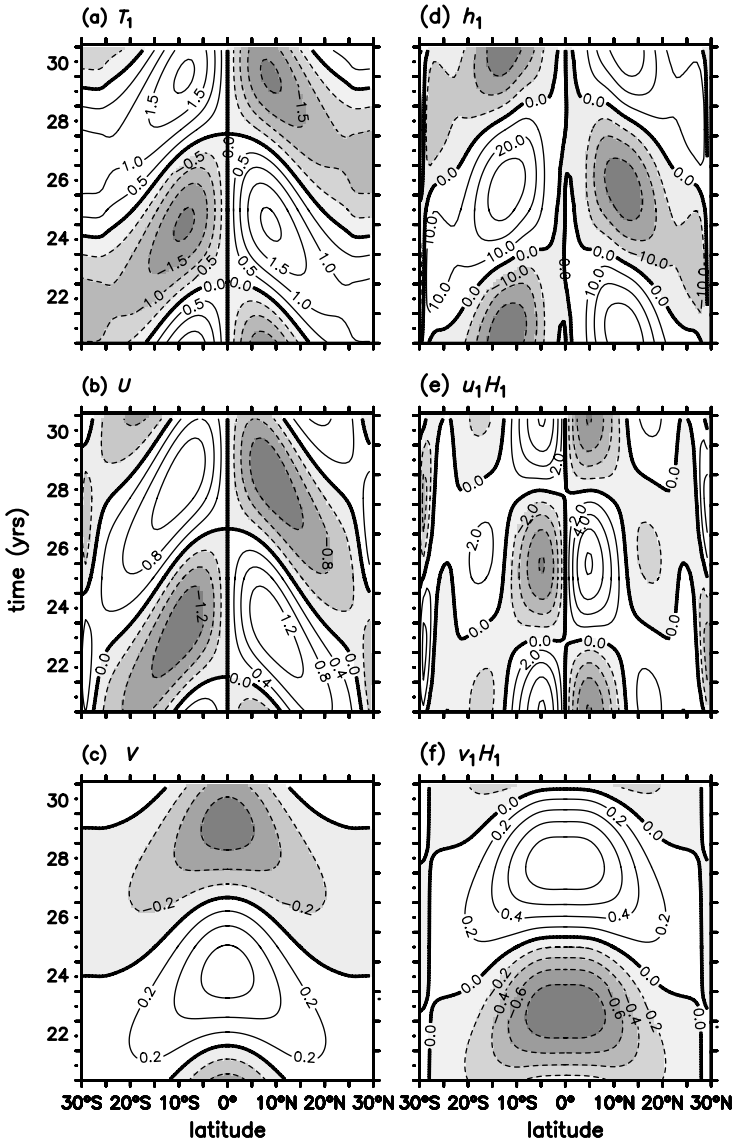

Figure 1. Case-1: Latitude-time structure of the zonally averaged (a) SST, (b) zonal wind, (c) meridional wind, (d) mixed layer depth, (e) zonal mixed layer transport and (f) meridional mixed layer transport anomalies. The unit is ^{o}C for the SST, ms^{-1} for the wind components, m for the mixed layer depth and m^{2}s^{-1} for the mixed layer transport components.

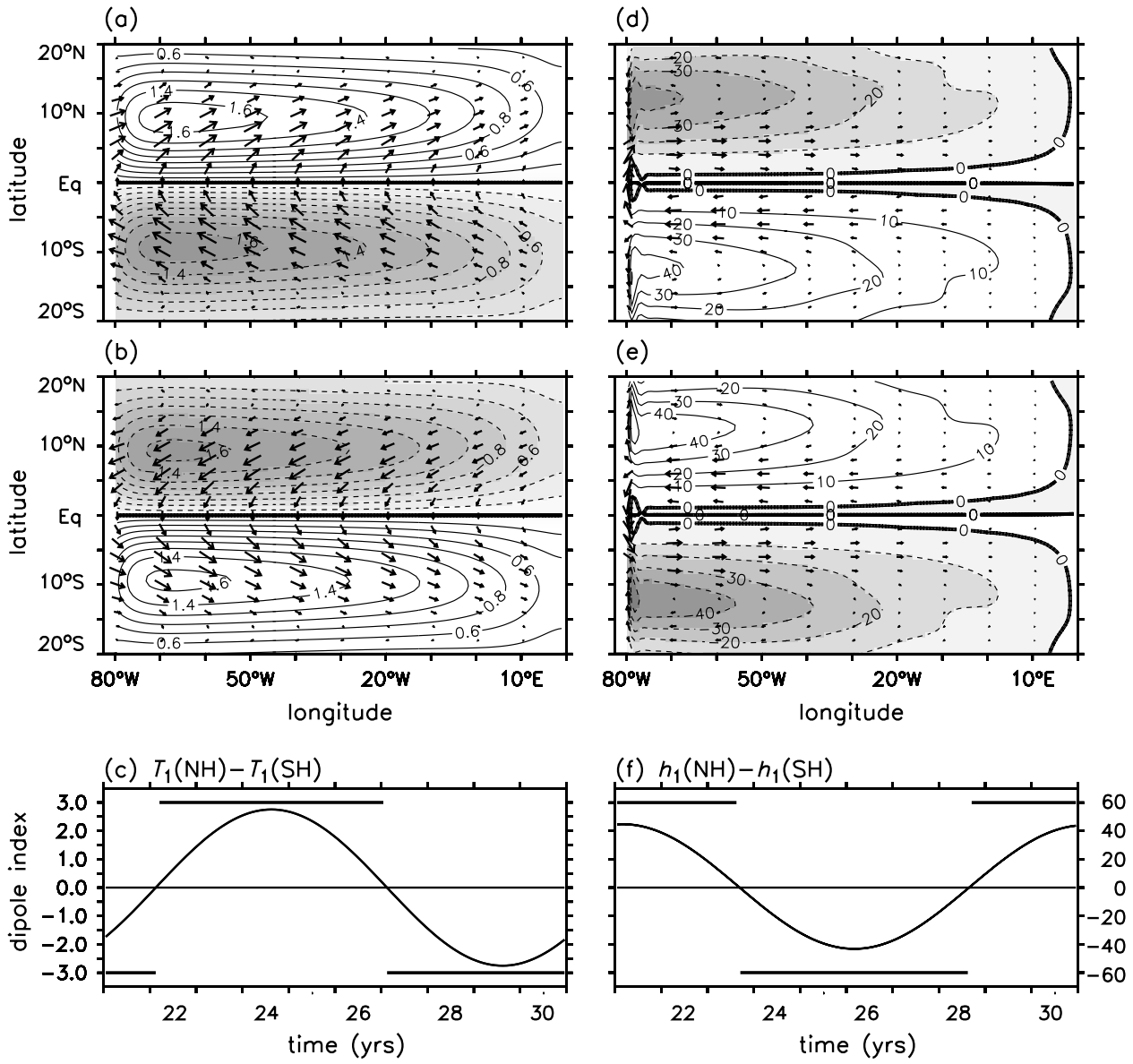

Figure 2. Case-1: Two-dimensional structure of SST and wind anomalies averaged for (a) the positive phase and (b) the negative phase are shown in the left column. The dipole index used for the phase averaging is the area-averaged SST of the northern hemisphere minus that of the southern hemisphere as shown in (c). The mixed layer depth and transport anomalies averaged for (d) the negative phase and (e) the positive phase are shown in the right column. The dipole index used in this case is the area-averaged mixed layer depth of the northern hemisphere minus that of the southern hemisphere as shown in (f). The maximum wind is about 1.3 ms^{-1}, and the maximum zonal mixed layer transport is about 9.5 m^2s^{-1}.

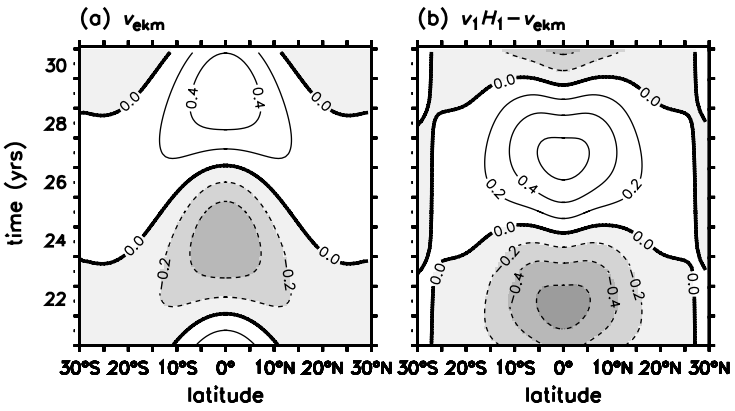

Figure 3. Case-1: Latitude-time structure of the zonally averaged meridional (a) Ekman transport and (b) non-Ekman transport components. The unit is m^2s^{-1}. Ekman transport is not defined at the equator, thus it is interpolated at the equator.

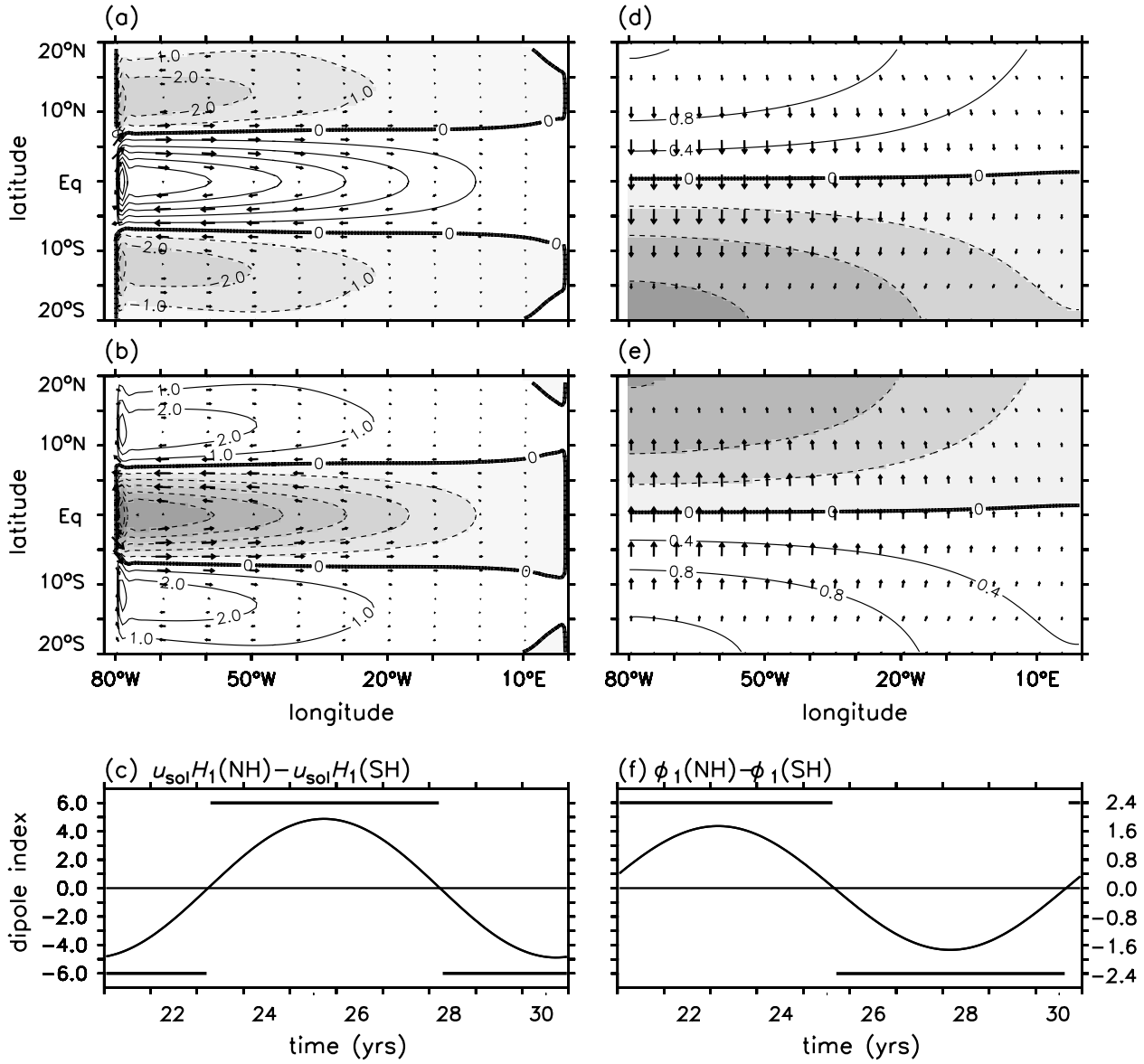

Figure 4. Case-1: The stream function (ψ_1) and solenoidal flow ($u_{sol}H_1$ and $v_{sol}H_1$) anomalies for the mixed layer averaged for (a) the positive phase and (b) the negative phase are shown in the left column. The dipole index used for the phase averaging is the area-averaged zonal solenoidal transport ($u_{sol}H_1$) of the northern hemisphere minus that of the southern hemisphere as shown in (c). The transport potential (ϕ_1) and potential flow ($u_{pot}H_1$ and $v_{pot}H_1$) anomalies for the mixed layer averaged for (d) the positive phase and for (e) the negative phase are shown in the right column. The dipole index used in this case is the area-averaged transport potential anomaly of the northern hemisphere minus that of the southern hemisphere as shown in (f). The unit is 10^{-6} m^3s^{-1} for the stream function and transport potential, and m^2s^{-1} for the solenoidal flow and potential flow components. The maximum transport value is about 9.4 m^2s^{-1} for the solenoidal flow component, and about 0.9 m^2s^{-1} for the potential flow component.

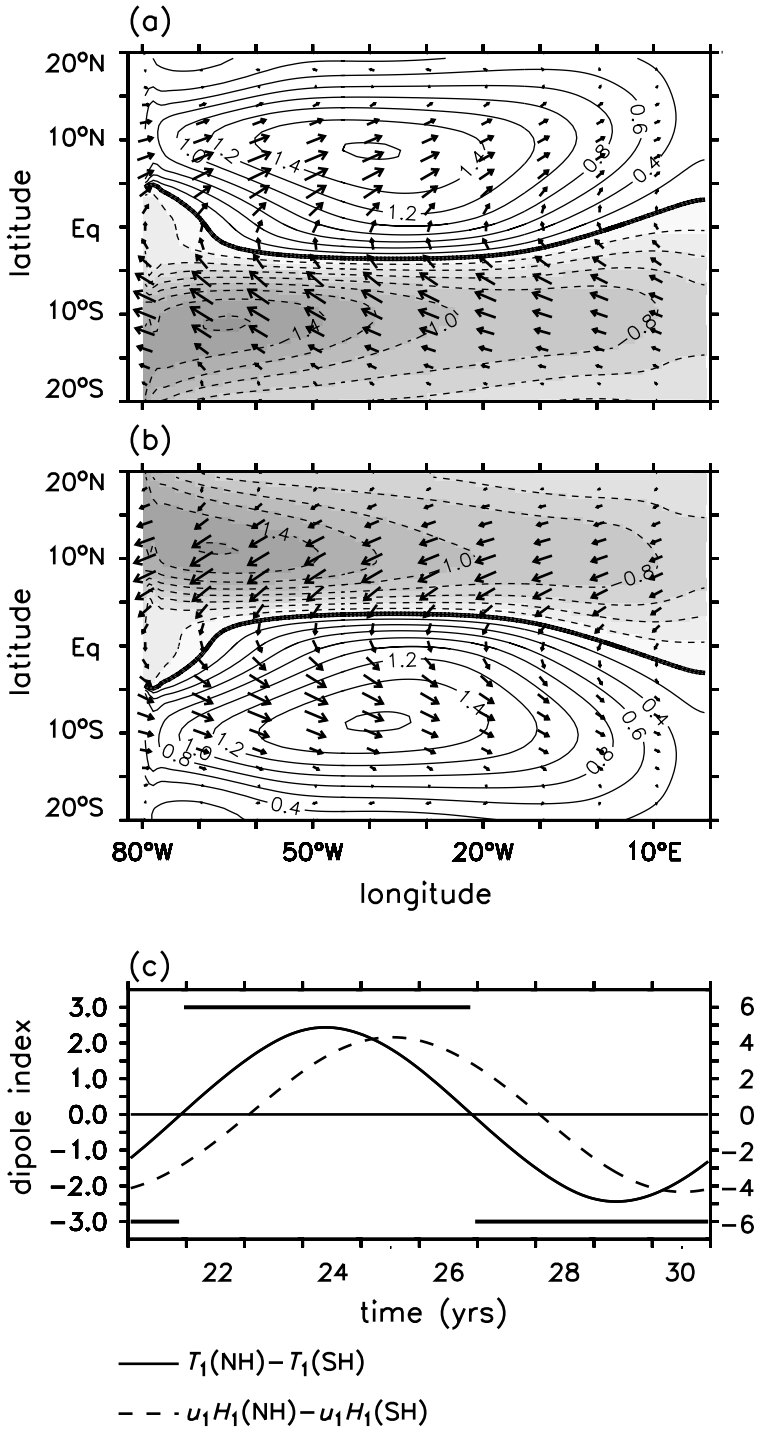

Figure 5. Case-2: Two-dimensional structure of SST and wind anomalies averaged for (a) the positive phase and (b) the negative phase. The dipole index used for the phase averaging is the area-averaged SST of the northern hemisphere minus that of the northern hemisphere as shown in (c). The broken line in (c) is the area-averaged zonal transport of the northern hemisphere minus that of the southern hemisphere, and this index is used for cross-equatorial gyre circulation: a negative value indicates a cyclonic circulation and a positive value indicates a clockwise circulation. The maximum wind is about 1.3 ms^{-1}.

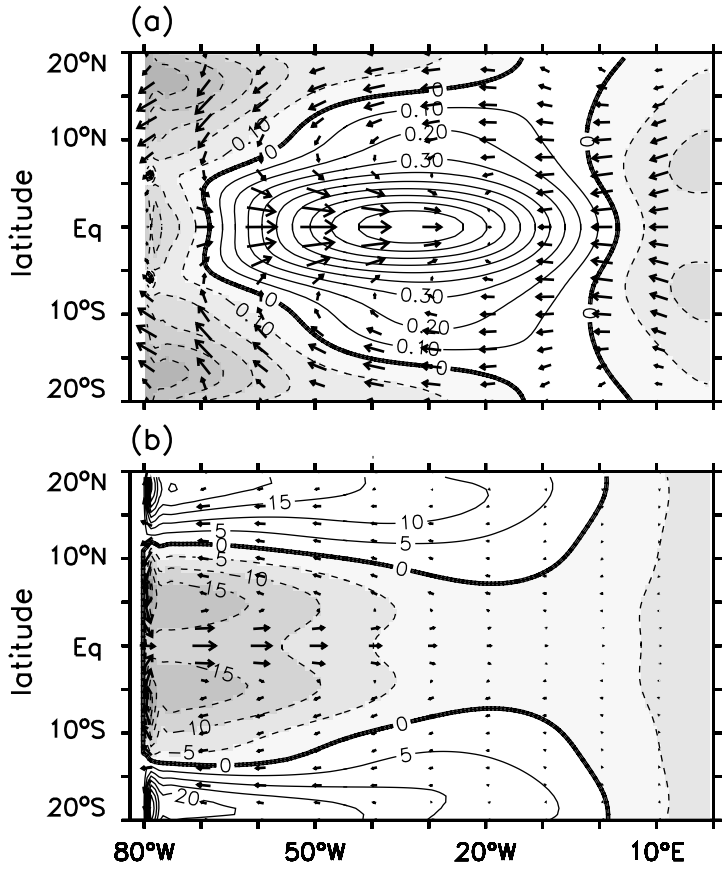

Figure 6. Case-2: The two-dimensional structures of (a) SST and wind anomalies, and (b) the mixed layer depth and transport anomalies, all averaged for one full cycle of the dipole oscillation between the model year 21 and 30. The maximum wind is about 0.4 ms^{-1}, and the maximum zonal mixed layer transport is about 3.2 m^2s^{-1}.

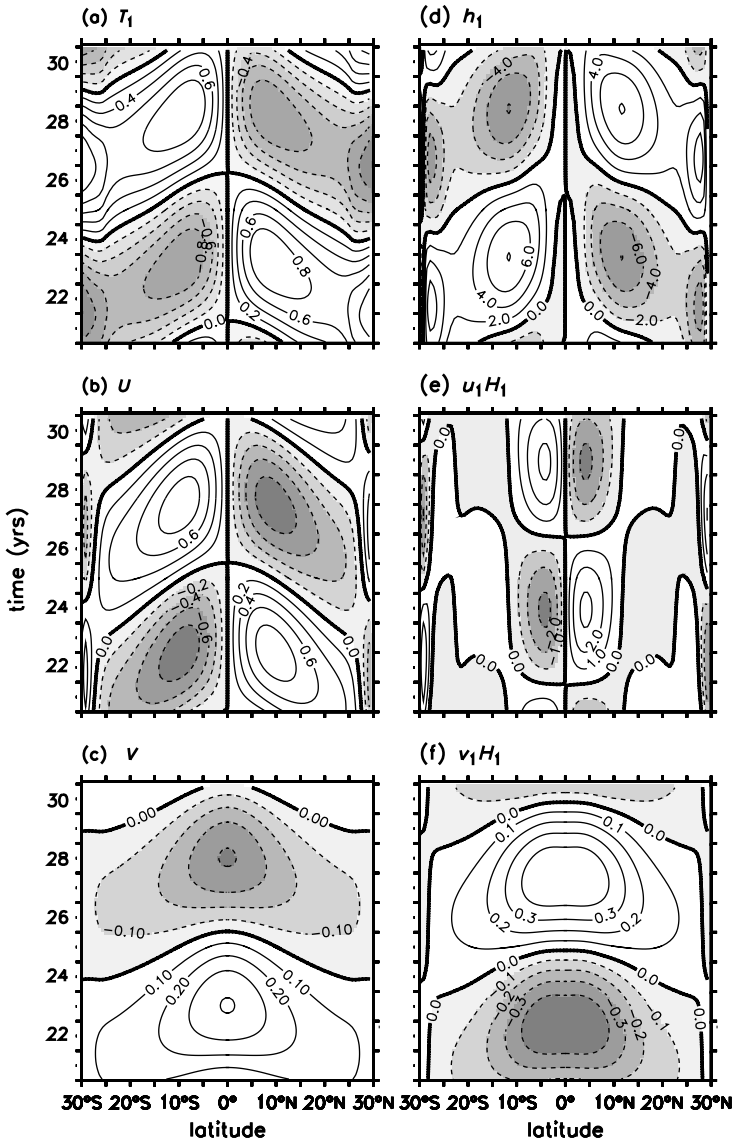

Figure 7. Same as in Fig. 1 but for Case-3. Note that the contour intervals are different from those used in Fig. 1.

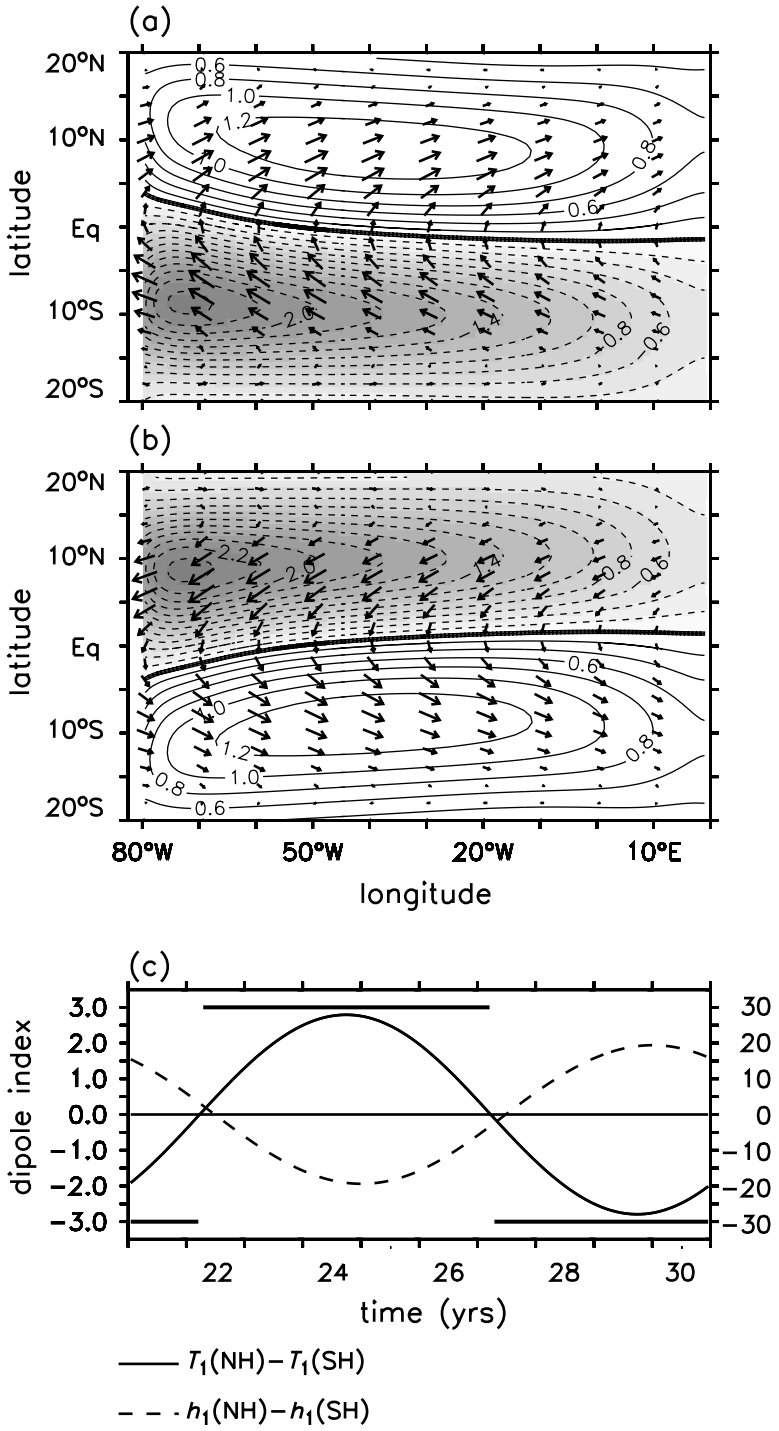

Figure 8. Same as in the left column of Fig. 2 but for Case-4. The broken line in (c) is the area-averaged mixed layer depth of the northern hemisphere minus that of the southern hemisphere. The maximum wind is about 1.4 ms^{-1}.

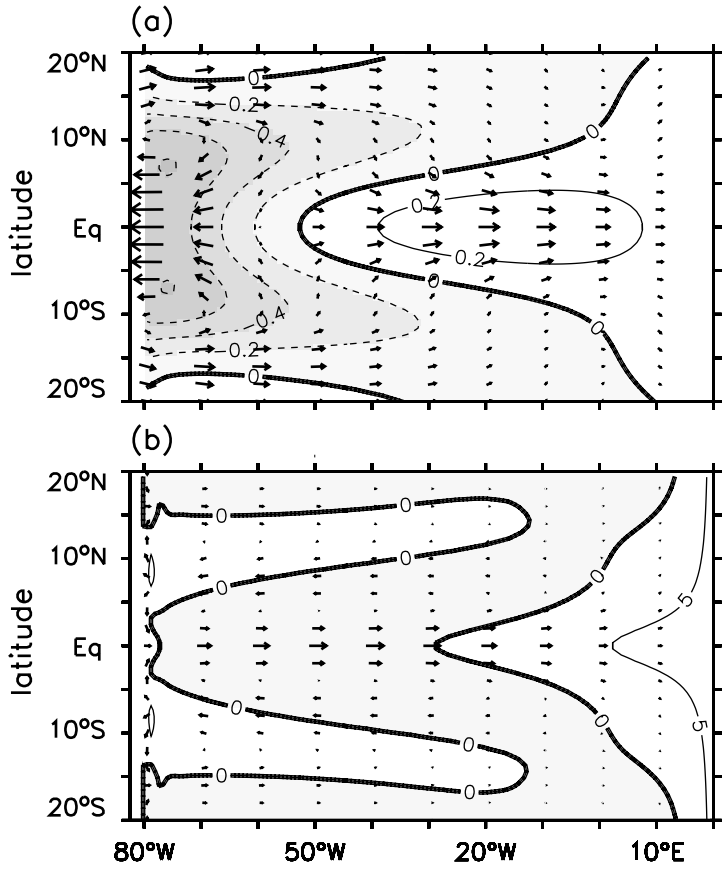

Figure 9. Same as in Fig. 6 but for Case-4. The maximum wind is about 0.3 ms^{-1}, and the maximum zonal mixed layer transport is about 2.5 m^2s^{-1}.

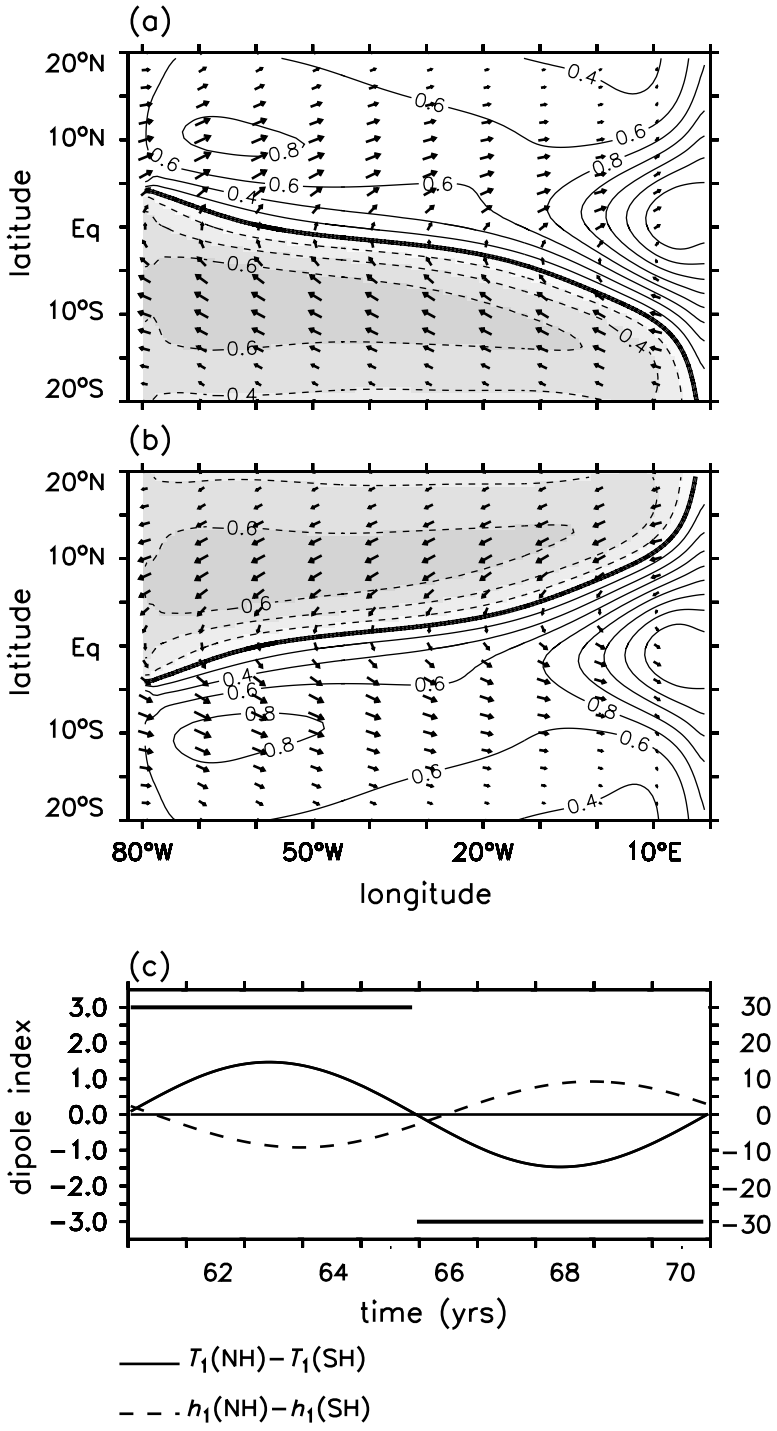

Figure 10. Same as in Fig. 8 but for Case-5. The maximum wind is about 0.8 ms^{-1}.

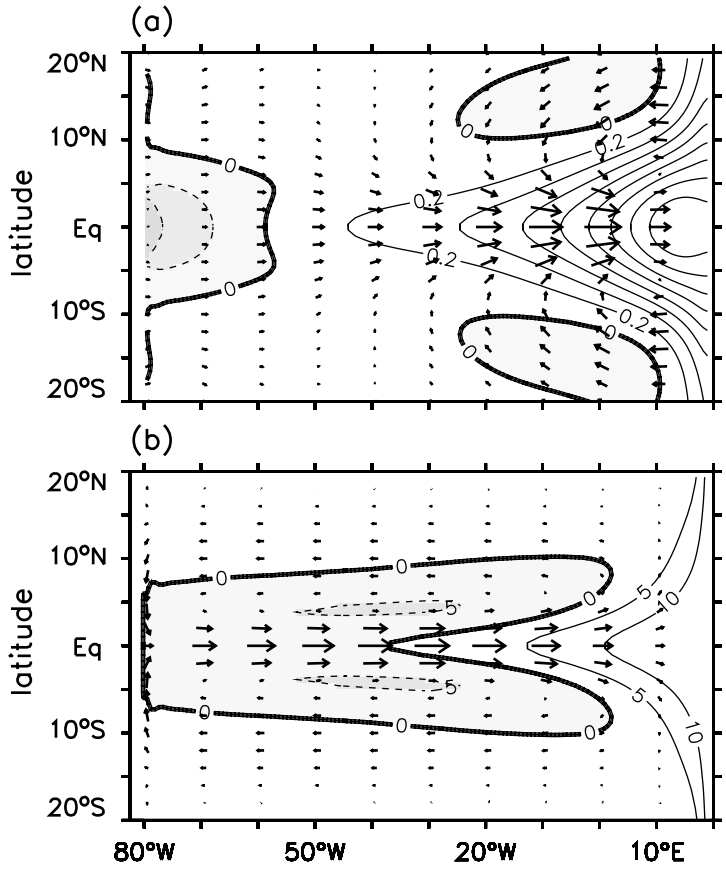

Figure 11. Same as in Fig. 9 but for Case-5. The maximum wind is about 0.4 ms^{-1}, and the maximum zonal mixed layer transport is about 5.2 m^2s^{-1}.

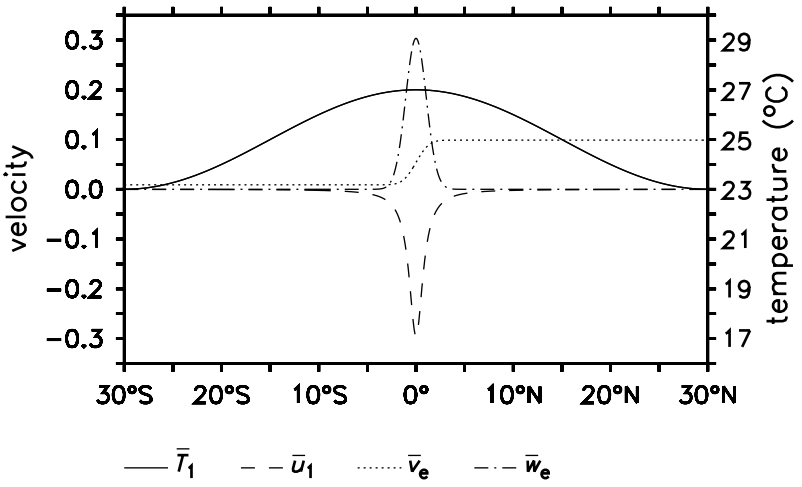

Figure 12. The mixed layer temperature (^oC), zonal mixed layer velocity (in m s^{-1}), meridional mixed layer velocity (in 10 m s^{-1}) and entrainment rate (in 10^5 m s^{-1}) of the mean state used for Case-6 and Case-7. See text for how these values are derived.

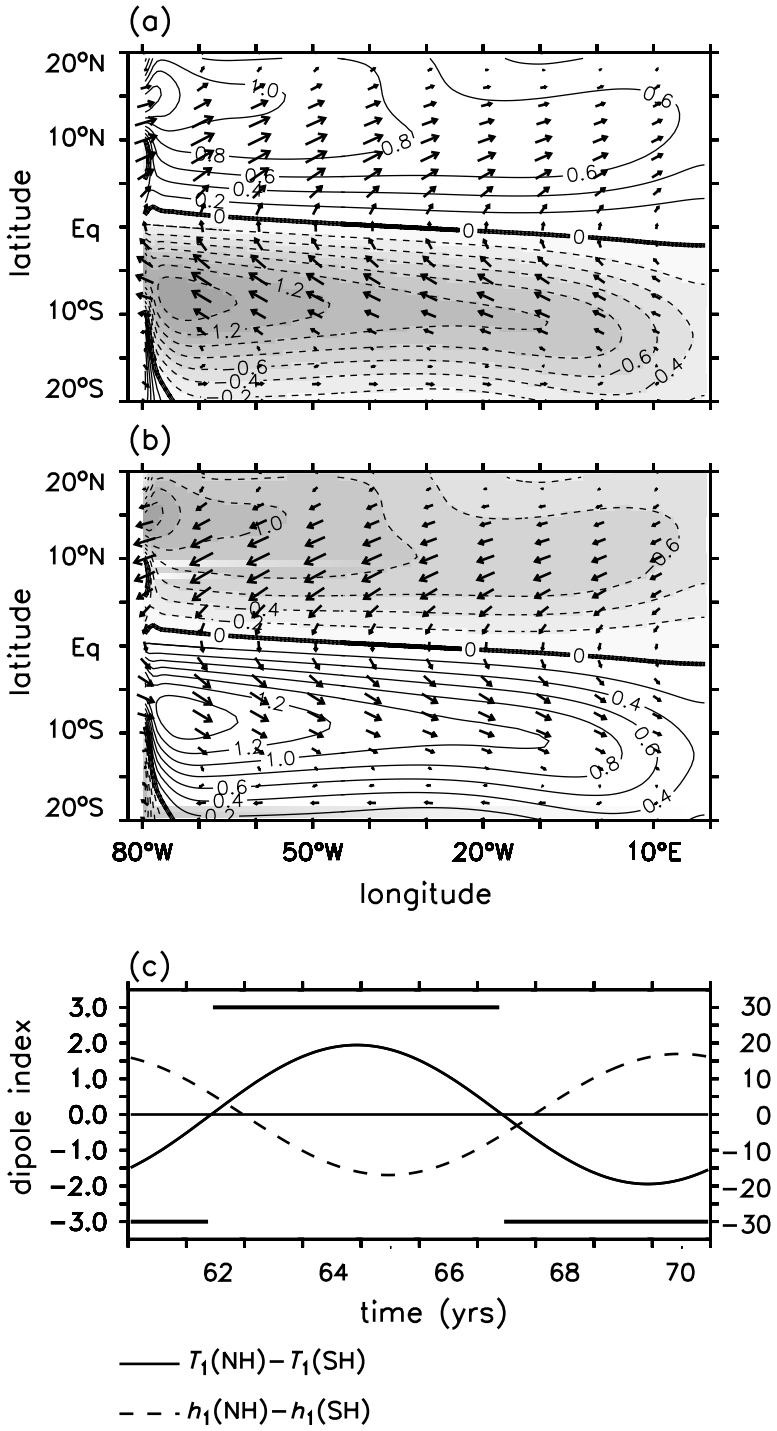

Figure 13. Same as in Fig. 8 but for Case-6. The maximum wind is about 1.2 ms^{-1}.

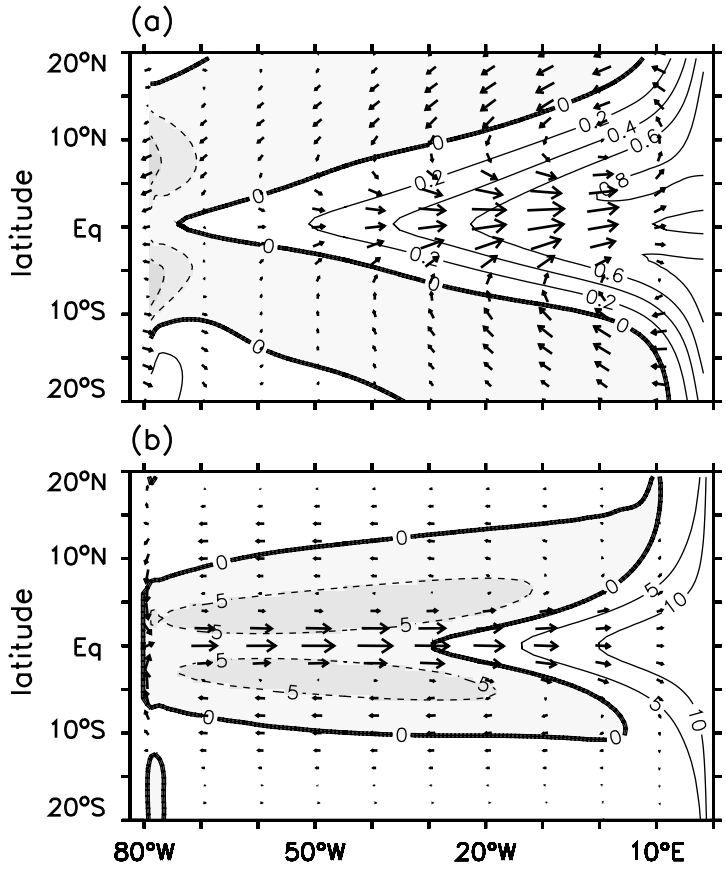

Figure 14. Same as in Fig. 9 but for Case-7. The maximum wind is about 0.4 ms^{-1}, and the maximum zonal mixed layer transport is about 5.3 m^2s^{-1}.

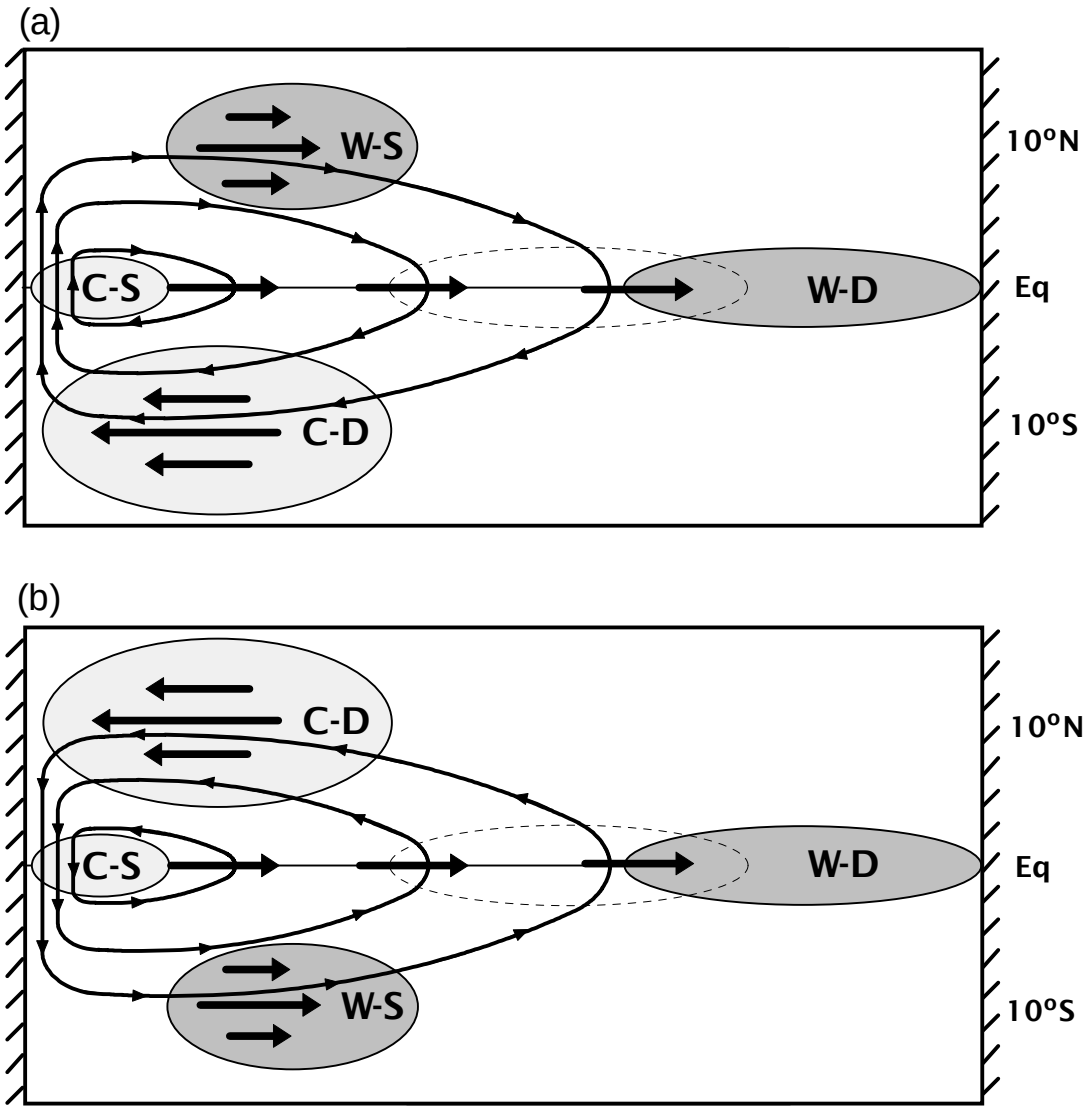

Figure 15. Sketch of the mechanism by which the positive zonal SST gradient is induced along the equator during (a) the positive and (b) negative phases of the Atlantic dipole oscillation. Thicker arrows indicate wind perturbations associated with the dipole oscillation. Dark shades are used for warm SST anomalies and light shades for cold SST anomalies. W-D represents a warm and deep anomaly; W-S a warm and shallow anomaly; C-D a cold and deep anomaly; and C-S a cold and shallow anomaly. Closed circuits represent cross-equatorial gyre circulation that brings the tropical surface water toward the equator. This gyre circulation supplies cold water in the western boundary layer and warm water in the Sverdrup interior during both the positive and negative phases of the dipole oscillation. The warm equatorial SSTA is then shifted to the east and intensified as a result of the Bjerknes feedback, thus, producing a stationary Atlantic-Niño condition.